Enhancing digital elevation models for hydraulic modelling using flood frequency detection

Ettritch, Georgina; Hardy, Andrew; Bojang, Landing; Cross, Donall; Bunting, Peter; Brewer, Paul

Published in:
Remote Sensing of Environment

DOI:
10.1016/j.rse.2018.08.029

Publication date:
2018

Citation for published version (APA):
Ettritch, G., Hardy, A., Bojang, L., Cross, D., Bunting, P., & Brewer, P. (2018). Enhancing digital elevation models for hydraulic modelling using flood frequency detection. *Remote Sensing of Environment*, *217*, 506-522. https://doi.org/10.1016/j.rse.2018.08.029

Remote Sensing of Environment 217 (2018) 506–522

Contents lists available at ScienceDirect

Remote Sensing of Environment

journal homepage: www.elsevier.com/locate/rse

Enhancing digital elevation models for hydraulic modelling using flood frequency detection

Georgina Ettritch[a,*], Andy Hardy[a], Landing Bojang[b], Dónall Cross[c], Peter Bunting[a], Paul Brewer[a]

[a] Department of Geography and Earth Sciences, Aberystwyth University, Aberystwyth, United Kingdom
[b] Department of Water Resources, the Gambia
[c] Institute of Biological, Environmental and Rural Sciences, Aberystwyth University, Aberystwyth, United Kingdom

ARTICLE INFO

Keywords:
Digital elevation model
DEM
SRTM
Flood modelling
River Gambia
Landsat

ABSTRACT

Medium-resolution DEMs have limited applicability to flood mapping in large river systems within data sparse regions such as Sub-Saharan Africa. We present a novel approach for the enhancement of the SRTM (30 m) Digital Elevation Model (DEM) in The Gambia, West Africa: A time-series analysis of flood frequency and land cover was used to delineate differences in the vertical limits between morphological units within an alluvial floodplain. Combined with supplementary river stage data and vegetation removal techniques, these methods were used to improve the estimation of bare-earth terrain in flood modelling applications for a region with no access to high-resolution alternatives. The results demonstrate an improvement in floodplain topography for the River Gambia. The technique allows the reestablishment of small-scale complex morphology, instrumental in the routing of floodwater within a noise-filled DEM. The technique will be beneficial to flood-risk modelling applications within data sparse regions.

1. Introduction

In data sparse regions (such as sub-Saharan Africa), hydraulic flood modelling applications are limited to the use of medium-resolution (~30 m) Digital Elevation Models (DEMs) including the Shuttle Radar Topography Mission (SRTM: NASA JPL), ASTER Global DEM (GDEM: NASA JPL), and most recently, the ALOS Global Digital Surface Model (AW3D30: JAXA). These products have been implemented within 1D/2D flood modelling applications across large river reaches (typically exceeding 10,000 km^2 in domain extent) to basin-scale and region-scale analysis (covering multiple basins) (e.g. da Paz et al., 2011; Neal et al., 2012; Wilson et al., 2007; Biancamaria et al., 2009; Amarnath et al., 2015; Lewis et al., 2013). A large domain extent requires the resampling of DEM data at coarser resolution (e.g. through mean pixel aggregation) or the use of low-resolution data (e.g. Biancamaria et al., 2009) to reduce the computational demand on flood model performance (Amarnath et al., 2015) (Table 1). Increasing computational efficiency through coarse resolution resampling is particularly important for large-scale rivers, where flood pulses are extensive not just in space, but also in time (da Paz et al., 2011).

Coarse resolution resampling can, in itself, be viewed as a DEM enhancement technique: SRTM, as the most commonly used product in large-scale flood modelling and the primary subject of this investigation, contains a high level of pixel-to-pixel noise, known as the short-wave error component (Rodriguez et al., 2006). The smoothing effect of pixel aggregation works to lower the vertical error margin of the DEM relative to the vertical range of floodplain morphology and flood wave amplitude (e.g. Wilson et al., 2007; Neal et al., 2012). Recent improvements in hydraulic modelling have been made specifically in relation to large-scale flood mapping at resolutions below the native grid spacing of a DEM. For example, the development of the sub-grid channel mode in LISFLOOD-FP allows the inclusion of channel geometry at the sub-grid level. As such, DEM resolution for the 2D component can be coarsened without impacting upon the representation of channel flow in the 1D component (Neal et al., 2012; Lewis et al., 2013).

However, care must to be taken to ensure that DEM coarsening is not detrimental to model performance, particularly when floodwater routing is controlled primarily by floodplain topography. For example, DEM aggregation has been found to lead to the eradication of key regions of riparian floodwater storage, fundamental to the accurate simulation of flood wave travel time (Horritt and Bates, 2001). Pixel aggregation has also been found to limit processes of floodplain dewatering and the representation of low water inundation extent

* Corresponding author.
E-mail addresses: gee25@aber.ac.uk (G. Ettritch), ajh13@aber.ac.uk (A. Hardy), dec8@aber.ac.uk (D. Cross), pfb@aber.ac.uk (P. Bunting), pqb@aber.ac.uk (P. Brewer).

https://doi.org/10.1016/j.rse.2018.08.029
Received 7 October 2017; Received in revised form 23 August 2018; Accepted 24 August 2018

Table 1
Examples of the use of medium to low-resolution DEMs in flood modelling and associated resampling of raster-based elevation data relative to model domain extent.

Study	DEM	Original (m)	Resampled (m)	Domain (km^2)	Scale
Neal et al. (2012)	SRTM	90	905	210,389	Sub-basin
Wilson et al. (2007)	SRTM	90	270	13,000	Sub-basin
Biancamaria et al. (2009)	ACE	1000	1000	790,000	Sub-basin
da Paz et al. (2011)	SRTM	90	2000	219,514	Sub-basin
Komi et al. (2017)	SRTM	30	30–960	72,000	Basin
Lewis et al. (2013)	SRTM	90	900	223,000	> Basin
Sampson et al. (2015)	SRTM	90	1000	–	Global

through the removal of complex, small-scale topography (Wilson et al., 2007). Overall, optimal DEM resolution is a compromise between: 1) Accounting for flood wave amplitude and the complexity of floodplain topography (e.g. Wilson et al., 2007), 2) The vertical accuracy of the DEM relative to the above and 3) Optimising computational efficiency of the flood model relative to study domain extent and flood wave temporality.

1.1. Methods of DEM enhancement

The relative/absolute vertical error of medium-resolution DEMs (e.g. SRTM with an absolute vertical error > 5 m in regions with slopes of < 10° (Gorokhovich and Voustianiouk, 2006)) will often exceed the vertical range in floodplain morphology and flood wave amplitude. Therefore, medium-resolution DEMs are often considered to be unsuitable for use in the modelling of overbank flow controlled by floodplain topography, without modification (Bates, 2012). Furthermore, large river systems contain complex flow networks that control the routing of water/sediment across the floodplain (Lewin and Ashworth, 2014). Many small-scale features instrumental in floodwater routing will be missed by medium-resolution DEMs in the first instance, a problem exacerbated further by coarse resolution resampling, as outlined above. In addition, the presence of closed canopy vegetation, such as mangrove forests, can mask the bare earth terrain below (Sun et al., 2003; Yastikli et al., 2006; Tighe and Chamberlain, 2009). This is problematic for the majority of large tropical floodplains where vegetation cover is often dense, continuous and does not experience the leaf-off conditions typically associated with winter months in temperate regions. As such, an estimate of bare-earth terrain under vegetation using Earth Observation data is limited. Tidally-influenced tropical regions are particularly problematic as saline-tolerant species will persist throughout the hydrological year and may experience only limited periods of die-off and subsequent exposure of the underlying surface. The following literature review is a brief account of techniques available to the end-user for the enhancement of SAR-based or optical-based elevation data.

Common DEM enhancement techniques include data fusion (i.e. hybridisation), waterbody masking, void filling, stream burning and vegetation removal. Data fusion is typically conducted at the landscape-scale. For example, SRTM can be fused with ASTER GDEM to capitalise on the relative differences in sensor performance over mountain slopes, valleys and floodplains for respective SAR and optical-derived DEMs (e.g. Tran et al., 2014). However, this technique has also been effective at improving topography within the floodplain. For example, 2.5 m Cartosat-1 data (Patel et al., 2016) was combined with 90 m SRTM data to form an 8 m hybridised DEM that compensated for the limited performance of the Cartosat-1 DEM over paddy fields (Sanyal et al., 2014).

InSAR-derived DEMs such as SRTM produce a noisy water surface with a high density of data voids due to the specular reflection of C-Band microwave energy over water (Lehner et al., 2008) and side-looking angles of spaceborne/airborne radar systems. Waterbody masking applies a constant elevation value over an open water surface and allows the removal of elevation anomalies and data voids associated with these regions. SRTM has been improved at global-scale through the use of the auxiliary water mask: SWBD (SRTM Water Body Data). A similar dataset AWBD (ASTER Water Body Dataset) has also been applied to GDEM version 3 (Abrams, 2016).

Data voids are negative relief features of internal drainage that include single-cell/double-cell sinks and larger regions. These features are easily resolvable using common fill techniques that raise the elevation of an internally draining region to the level of its peripheral pour point (e.g. Jenson and Domingue, 1988; Planchon and Darboux, 2001; Wang and Liu, 2006). Fluvial erosion generally dictates a hydrologically connected landscape (Wang and Liu, 2006; Mark, 1988) suggesting that the majority of such features are erroneous and should be eliminated from the topographic profile (Mark, 1988; Senevirathne and Willgoose, 2013; Lindsay and Creed, 2005a, 2005b). However, larger features may in fact be natural regions of negative relief (e.g. de Carvalho Junior et al., 2014; Siart et al., 2009; Smith et al., 2013). In a fluvial context, negative relief formations may include: palaeochannels, riparian lagoons and pools, that will remain inundated following floodwater recession (Lewin and Ashworth, 2014; Smith et al., 2013). Removal of these features may contribute to inaccuracies in the calculation of floodwater storage within the floodplain. Some negative relief features that are hydrologically connected to the main trunk stream maybe inaccurately presented as internally draining features. In such cases, a breaching algorithm (e.g. Martz and Garbrecht, 1999) can be used to eliminate anomalous topographic highs and allow hydrological reconnection.

Stream burning also facilitates a hydrologically connected surface within a DEM, thereby, improving floodwater routing within a 2D hydraulic model. Depending on DEM resolution river channels may become disconnected or are too narrow to be detected as a negative relief feature in the first instance. Automated stream burning procedures (Lindsay, 2016) can directly modify channel elevation within a DEM, based on a predefined flow path. One example is the AGREE method for DEM surface reconditioning (Hellweger, 1997). The technique generates a trench along a given stream vector, while eliminating proximal parallel flow paths through a lateral smoothing procedure. In data sparse regions, streams are typically generated by lowering channel cells by a constant value (representative of predicted channel depth), relative to adjacent floodplain cells (representative of river bank height) (Lindsay, 2016). In doing so, the integrity of channel geometry estimation is inherently dependent upon the vertical accuracy of the DEM. If bank height above river bed is distorted by riparian vegetation cover, channel bed elevation, relative to local floodplain level will be overestimated.

Furthermore, in lowering channel cells by a constant value it is assumed that the DEM surface is representative of channel bed gradient in the first instance. However, this is unlikely to be the case, particularly within gently sloping regions where vertical error typically exceeds topographic variation within a DEM. As such, stream burning procedures often incorporate interpolation techniques that linearly recondition channel bed elevation between predetermined values in the downstream direction. For example, LISFLOOD-FP (1D/2D mode) applies linear interpolation between discrete cross-sections of known width and bed elevation. Using bank height as an approximation of channel depth, the estimated geometry is burned directly into the DEM,

along a predefined channel vector (Bates et al., 2013).

In general, stream burning techniques are limited to the width of a single cell. A single cell approach is useful in instances where channel width is equal to DEM resolution. As previously established, where channel width is below DEM resolution, a sub-grid approach to channel representation can be applied (Neal et al., 2012). However, instances in which channel width exceeds DEM resolution are more difficult to reconcile without access to a high-resolution bathymetric survey. This is because rivers display anisotropic behaviour (Merwade et al., 2006). Spatial heterogeneity in flow direction prevents the application of commonplace interpolation techniques (for example, Inverse Distance Weighting (IDW) or Kriging) for bed elevation estimation between discrete cross-sections in the downstream direction (Zhang et al., 2016; Merwade et al., 2008). Although, such techniques can be modified to allow a robust estimation of channel bathymetry in a data sparse environment (Merwade, 2009).

Vegetation removal techniques typically work by subtracting vegetation height from the surface profile using a uniform height value, spatially informed by forest boundary data (e.g. Coe et al., 2008; Paiva et al., 2011). However, the assumption here is that there is no spatial variation in inter-species height and that EMR (Electro-magnetic Radiation) is unable to penetrate the vegetation canopy (Wittmann et al., 2004). An alternative approach (particularly useful for SAR-based DEMs) is the subtraction of a uniform percentage height value that accounts for the partial penetration of the canopy by microwave radiation. For example, Wilson et al. (2007) subtracted 50% of height from the SRTM profile over vegetated areas, based on C-SAR canopy penetration depth. The study was spatially informed by a vegetation map of the study area (Hess et al., 2003). Using a global vegetation height dataset (Lefsky, 2010; Simard et al., 2011), Baugh et al. (2013) performed a sensitivity analysis on optimal percentage height removal for C-SAR data, concluding that 50–60% height removal facilitated the greatest improvement in flood prediction using LISFLOOD-FP for a region in the Amazon, correlating with results from Wilson et al. (2007). Recent improvements to vegetation removal have focused on the use of non-uniform correction values as a function of vegetation height and density at the global-scale (O'Loughlin et al., 2016; Yamazaki et al., 2017). Auxiliary datasets including: 1) MODIS-derived canopy density 2) ICESat altimetry data and 3) global vegetation distribution (Simard et al., 2011) have been combined to allow the level of height subtraction to vary by climatic zone and species (O'Loughlin et al., 2016). Overall, vegetation removal techniques will generally improve the vertical accuracy of a DEM, particularly regarding optical-stereo derived or X-band/C-band data.

1.2. Towards a geomorphological approach to DEM enhancement at floodplain-scale

With the exception of stream burning, enhancement techniques of medium-resolution DEMs focuses on the refinement of established topography rather than on resolving the omission of key geomorphological features. This is inherently problematic when attempting to model overbank flow controlled by complex floodplain topography. Large floodplains (typically 4–40 km in width) cannot be classed simply as the passive recipients of overbank flow and diffuse sediments (Lewin and Ashworth, 2014). These regions will often contain a complex network of ephemerally and permanently connected channels (Day et al., 2008; Trigg et al., 2012) and other features that are actively involved in the progression, storage and recession of floodwater. This study demonstrates the use of freely available auxiliary optical data for resolving the omission of geomorphological features, inherently involved in the routing of overbank flow within a DEM.

The use of both optical and/or radar satellite imagery (10–30 m) for the mapping of fluvial geomorphology has been successfully demonstrated (e.g. Lewin and Ashworth, 2014). Coupled with information on river stage, this presents a unique opportunity to enhance medium-resolution DEMs, enabling them to represent complex floodplain drainage network features for use in hydraulic flood modelling in data sparse regions. Specifically, the use of multi-temporal flood frequency analysis of satellite imagery (e.g., Pekel et al., 2016) can be used alongside classification of vegetation type (and a phenological understanding of their distribution with regards to surface water availability) to determine the spatiotemporal variance in the exposure of geomorphological landforms. In doing so, relative differences in elevation across the floodplain can be established as a function of river stage. This information can be used to correct a DEM in regions where the relative and absolute vertical error of a DEM exceeds the vertical range in floodplain morphology and flood wave amplitude.

1.3. Characterising the use of surface water mapping in DEM enhancement

By mapping water extent, floodplains can be segmented into geomorphological units, defined by their relative level of exposure above a given water surface height. For example, in tidally influenced reaches, areas of partially vegetated mudflats remain dry at high tide (e.g. White, 1983), while areas covered by halophytic vegetation indicate areas of lower elevation, flooded at high tide. The concept of using water extent to alter a DEM was first introduced by Mason et al. (2016) for the purpose of reducing random noise in the TanDEM-X WorldDEM (12.5 m) product. Mason's method is applied by removing outliers from the DEM and averaging the height of adjacent pixels along a waterline. Adjacent contours subsequently form upper and lower elevation boundaries and pixels between them can be constrained accordingly: pixel elevation that exceeds the upper flood limit is lowered to match it; pixel elevation below the lower contour limit is raised to the height of the waterline. This concept is founded upon the fact that water surface elevation changes slowly along a reach for large rivers; meaning therefore, that a waterline will reflect consistent elevation, and can be subsequently classed as a 'quasi-contour' for local DEM adjustment (Mason et al., 2016).

However, this method was designed specifically for shallow-sloping regions with short vegetation: Short vegetation reduces the potential for horizontal error in waterline extent detection within SAR imagery and elevation overestimation within the DEM, associated with emergent vegetation. In large tropical wetlands, flood waves are shallow and the water surface will typically be associated with dense, emergent vegetation cover. As such, the establishment of a distinct waterline feature using optical or SAR-derived imagery is problematic. Studies have shown the potential for the use of SAR data in detecting changes in water extent across vegetation using a multi-temporal analysis of backscatter response (e.g. Tanis et al., 1994; Kasischke and Bourgeau-Chavez, 1997; Kiage et al., 2005; Long et al., 2014) and/or by assessing phase difference between polarizations (e.g. Horritt et al., 2003; Lu and Kwoun, 2009). However, success of a SAR-based approach is dependent on: 1) wavelength relative to canopy penetration potential (i.e. whether a double-bounce backscatter response can be obtained from the water surface, dependant on canopy height, density and stem orientation) (Henderson and Lewis, 2008); and 2) a thorough understanding of land cover distribution and antecedent conditions within reference imagery.

Optical data is limited to the detection of open water regions only (e.g. Pekel et al., 2016). Emergent vegetation at the edges of open water may result in the underestimation of surface water extent. However, an understanding of plant phenology with regards to surface water distribution can be used to inform the enhancement of floodplain topography within a medium-resolution DEM. Hydrological controls on species composition at floodplain-scale are particularly prominent within low-lying tidal regions (Twilley, 1985). For instance, in The Gambia, West Africa, savannah woodlands are permanently dry (i.e. raised above the level of fluvial inundation), mangroves and other halophytic vegetation types will be semi-diurnally inundated by tides, and partially vegetated mudflats will remain largely dry, allowing for the establishment of vegetation with inundation occurring only during

extreme flood events. A spectral classification of species composition across a fluvio-tidal environment can therefore be used to rectify clear topographic boundaries within a noise-filled DEM.

1.4. Study aims

The aim of this study is to develop a hydrologically corrected DEM surface specifically designed for the modelling of flood event scenarios, controlled by floodplain topography. This aim is achieved by addressing the following objectives: a) Determine to what extent the spatio-temporal inundation dynamics of a large tidal floodplain can be detected using a multi-temporal archive of medium-resolution optical imagery and b) to demonstrate how differences in morphological exposure relative to river stage can be used to improve the vertical accuracy of the SRTM DEM.

2. Methods

2.1. Study area

The study was based on an 86 km reach of the lower River Gambia in West Africa (Fig. 1). Total domain extent was 1794 km^2. Beginning in the Fouta Djallon Highlands in Guinea (Bøgh et al., 2003), the river Gambia is one of eight large river systems in the region (length: 1100 km; drainage area: 77,000 km^2) (Leveque, 1995). The watercourse follows a classic tropical regime with one short wet season (June to October) and a significant proportion of the annual runoff (60–75%) being concentrated within mid-August to mid-October (Leveque, 1995). Approximately 525 km of the lower course is characterised by a low valley gradient (~0.013 m/km) resulting in a tidal regime which extends up to the Gambian-Senegalese border during the dry season (Berry et al., 1985). Daily minimum and maximum stage readings for the main channel at Balingho (2015–2016) (source: Department of Water Resources, The Gambia) demonstrates a diurnal tidal range which exceeds seasonal change as a result of increased upstream discharge (Fig. 2) (Louca et al., 2008). During the dry season, floodplain inundation frequency is semi-diurnal, with spatial limits determined by the extent of high spring tide. During the wet season, these spatial maximums fluctuate as a combined function of increased upstream discharge at flood tide (Berry et al., 1985).

The study reach is morphologically static due to the stabilising effect of riparian vegetation cover, characteristic of most fluvial wetland systems (e.g., Martinez and Le Toan, 2007). The region is inter-tidal containing a complex network of creeks (known locally as bolons) that route tidal water across the floodplain on a semi-diurnal basis. Floodplain substrate consists of clay-based alluvium (Guillard et al., 2004; Louca et al., 2008) supporting mangrove forest (including *Rhizophora* sp. and *Avicennia* sp.; Bøgh et al., 2007) and short herbaceous vegetation (≤2 m) including grasses *Paspalum*, sp., *Sporobulus* sp., sedges (seasonal spike-rush: *Eleocharis* sp.), perennial shrub (sea-purslane: *Sesvium* sp.) and tall reeds (*Cyperus papyrus*, *Phragmites karka*). Aquatic floating vegetation, predominantly *Nymphaea* sp. (water lillies) occurs seasonally over open areas of freshwater (Bøgh et al., 2003). Areas of permanently exposed sediment within the floodplain represent regions least likely to be tidally influenced (White, 1983).

2.2. Flood frequency analysis

In total, 99 Landsat scenes (1986–2016) (including Landsat 5; Landsat 7; and Landsat 8) were incorporated into a rule-based classification system (Fig. 3) to classify nine land cover types representing key hydrologically-driven land cover classes within the floodplain (Table 2). The purpose of incorporating 99 scenes was to determine average hydrological conditions at season-scale, within a morphologically stabilised reach. In doing so, the effect of extreme flood events with a long return period on land cover representation was minimised. Scenes were atmospherically corrected to surface reflectance using ARCSI (http://rsgislib.org/arcsi/) and were subsequently subset to the study reach. The rule-based system was largely based on thresholding using vegetation indices including the Normalised Difference Vegetation Index (NDVI) (Eq. (1)) for identifying difference in chlorophyll content or leaf 'greenness' (Hay et al., 1998) and the Normalised Difference Pond Index (NDPI) (Eq. (2)) which can discriminate turbid water bodies with high suspended sediment (typical of large river systems) from other land cover types (Vignolles et al., 2009). Vegetated or partially vegetated mudflats were delineated by a threshold on Landsat 7/8 panchromatic band as these areas tend to be brighter (typical pixel value (Digital Number) > 8000) in the green to near infrared regions of the spectrum compared to other land cover types. Thresholds were determined manually by calibrating against false colour composites of the original Landsat imagery.

$$NDVI = [NIR - RED]/[NIR + RED] \quad (1)$$

$$NDPI = [MIR-GREEN]/[MIR+GREEN] \quad (2)$$

Success of the classification with regards to flood frequency assessment relies on *a priori* knowledge of land cover and land use to determine whether vegetation boundaries represent true regions of topographic change, or merely reflect a change from emergent to submerged vegetation, leaf-on to leaf-off conditions or the seasonal cultivation of cropland across relatively flat land. For example, tidally-influenced rice fields will change seasonally, transitioning to open water prior to initial growth stages and following harvesting (Carney, 1998a, 1998b). Whereas, the reduction in panchromatic brightness across bare mudflats suggests the encroachment of surface water. Peripheral rice fields are pluvially-fed and will dry out during the dry season as they are above tidal influence and persistent groundwater saturation (Fillinger et al., 2009). Inaccuracies in water extent prediction in the presence of floating aquatic vegetation must also be considered. The rule-based classification shown in Fig. 3 was designed specifically to account for these expected variations.

The resulting land cover map was used to determine variation in inundation extent at the sub-daily to seasonal scale based on the inundation characteristics associated with each land cover class (summarised in Table 2). Table 3 shows the total number of scenes available for each month. No data were available for wettest months, August and September due to extensive cloud cover.

The classification system was implemented in ERDAS Imagine (Version 2014). Classification accuracy was assessed through an error matrix using 1800 points with reference to high-resolution imagery (February 2016) in Google Earth Pro (version 7.1.5) and a panchromatic ALOS PRISM mosaic consisting of four individual scenes, covering the dry season (February 2010/2011) (provided by ESA). Each class was initially designated with 200 points, randomly spatially distributed using stratified random sampling. Ground-truth points were subsequently compared to land cover as predicted by the multi-temporal classification. Due to their narrowness, creeks (i.e. bolons) and drainage channels (of 15–30 m in width) were manually digitised within the classification and therefore excluded from the error matrix.

Each class represents a unique geomorphological unit with distinct spatiotemporal differences in inundation. However, from a non-temporal perspective there is significant overlap between some of these regions: Rice fields form a managed agricultural landscape but, swamp rice is also a saline tolerant species, spectrally similar to, and spatially concurrent with wild, unmanaged halophytic vegetation. Mudflats, whether ephemerally dry or permanently dry, consist of bare alluvial sediments raised above the local level of the densely vegetated floodplain. The main channel of the River Gambia and its tributaries remain hydrologically connected throughout the year and therefore represent regions of permanent water. For simplicity, distinct geomorphological classes with spectral similarities were merged to form five sub-categories (Table 4).

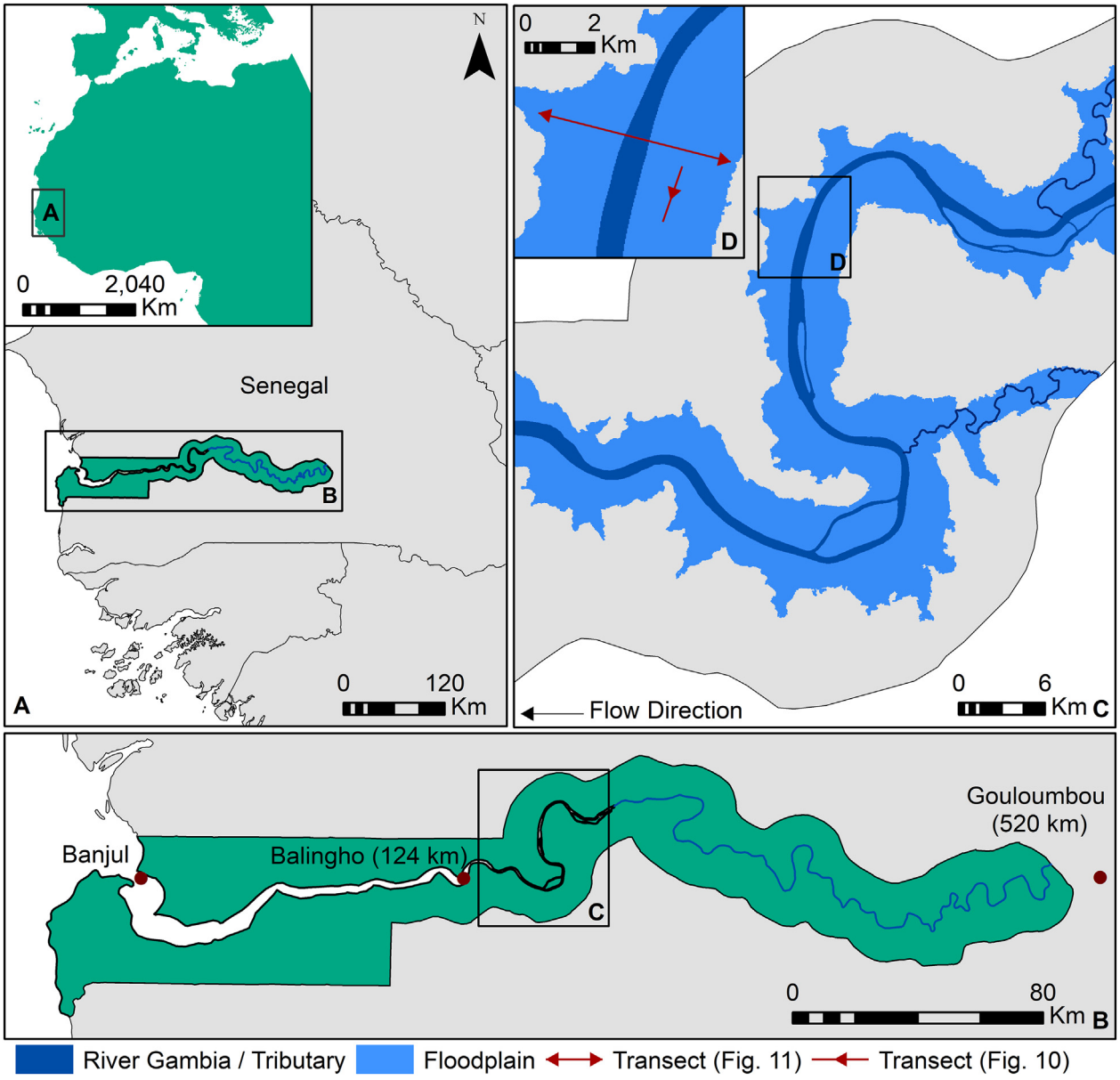

Fig. 1. Study Area in The Gambia, West Africa (values given in panel B) represent distance upstream (km) of gauging stations (red markers) from river mouth at Banjul. Panel C shows the specific location of the study area. Panel D shows the location of cross-sections for Figs. 10 and 11. (For interpretation of the references to colour in this figure legend, the reader is referred to the web version of this article.)

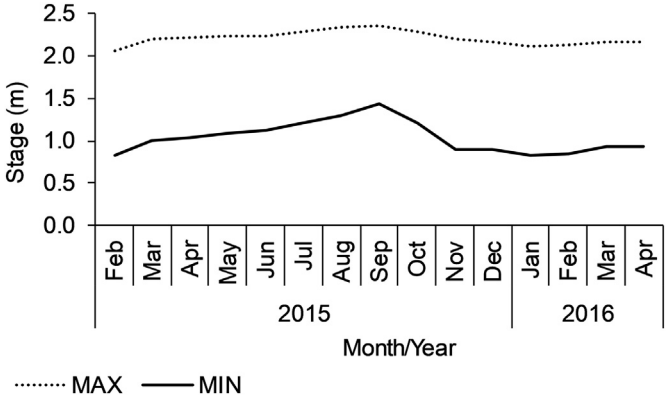

Fig. 2. Month-averaged high (MAX) and low (MIN) stage (metres above sea level) at Balingho gauging station (2015–2016).

2.3. DEM enhancement

The flood frequency product was used to modify and enhance 1-second arc SRTM DEM. The enhancement procedure is divided into two primary work packages outlined below (summarised in Fig. 4).

2.4. Work package 1: vegetation removal

Prior to the implementation of a hydro-geomorphologically corrected DEM, the influence of vegetation height noise within the intertidal zone was reduced. Studies have shown that C-band InSAR (used to generate the SRTM DEM) is capable of penetrating to within ~50% of the total canopy height (Kreiselmeier, 2015; Baugh et al., 2013). However, penetration potential is dependent on species- specific variations regarding canopy height and density (O'Loughlin et al., 2016). Within the Gambia study site, mangrove stands, and halophytic vegetation have a clear influence on the DEM. Average height for *Rhizophora* sp. is 20 m along the north bank within the study region (Twilley,

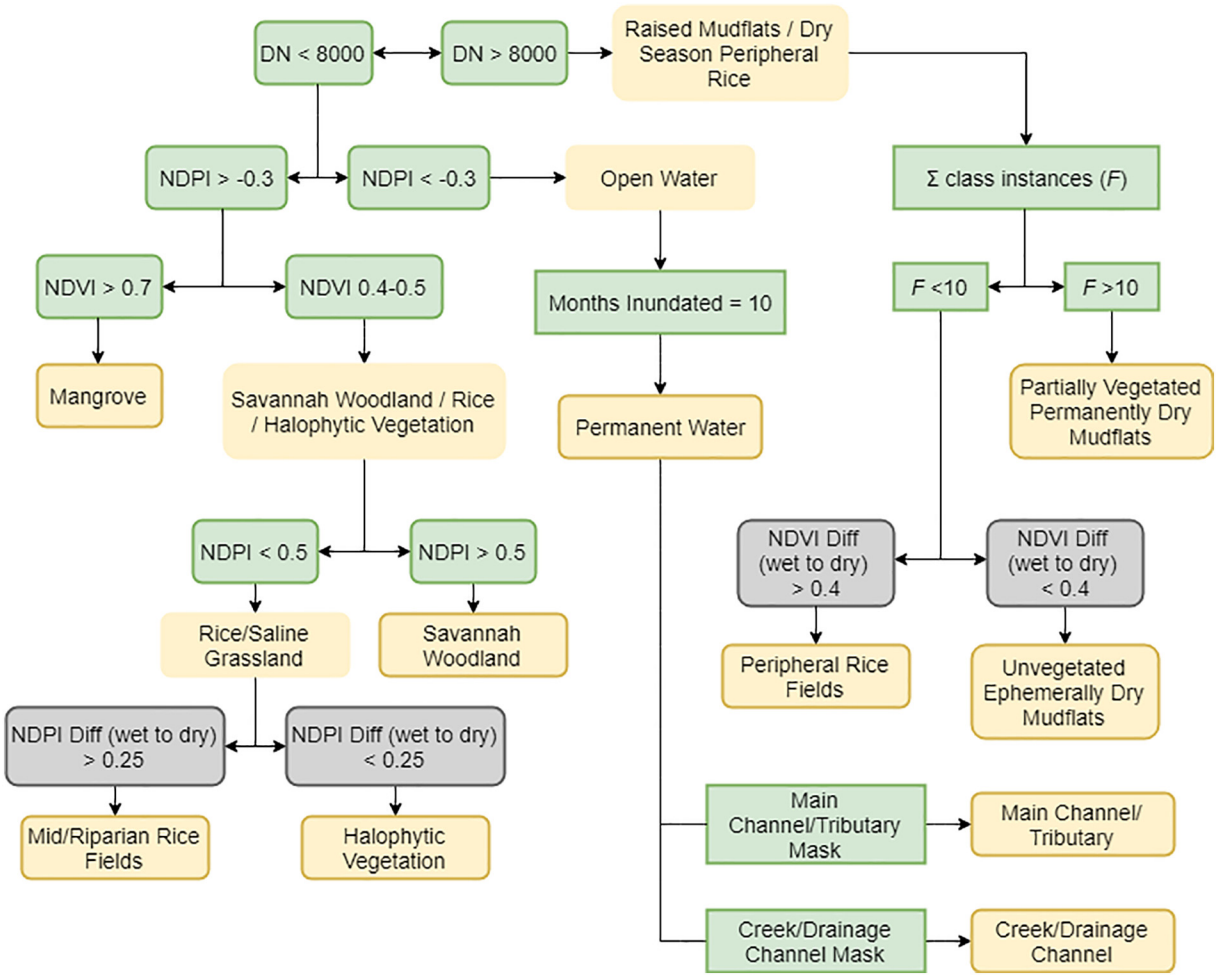

Fig. 3. Rule-based decision tree of land cover classification applied to Landsat imagery (Values represent typical thresholds relating to NDVI, NDPI, seasonal differences and summed incidence; DN (Digital Number) refers to Panchromatic Brightness).

1985). Halophytic vegetation (considering sedges, tall reeds and grasses) has an average height of ~2 m (Twilley, 1985).

Without auxiliary ground data it is not possible to establish penetration depth of C-band radar over vegetation. As such, a penetration potential of 50% was selected for both mangrove and halophytic vegetation. Although relatively optimistic (particularly regarding the dense canopy structure of mangroves) this value is in agreement with the penetration potential of other dense, fluvially-influenced vegetation types across tropical wetlands (e.g. Wilson et al., 2007). Per-pixel elevation was reduced by a respective 10 m across mangroves (reflective of the dominance of tall, *Rhizophora* sp. with a mean height of 20 m) and 1 m across halophytic vegetation (assuming that short halophytic vegetation will be ~2 m in height). The aim of the procedure is not to increase the absolute/relative vertical accuracy of bare-earth terrain across halophytic vegetation and mangrove as mutually exclusive vegetative units. Its purpose is to improve the relative vertical accuracy *between* these units and the subsequent routing of water within the inter-tidal zone.

Table 2
Land cover classes and associated inundation dynamics.

Class	Description	Return period	Classification feature
Halophytic vegetation	Tidally-influenced, short herbaceous vegetation	< 1 day to 14 days	NDVI
Mangrove	Tidally influenced mangrove forest	< 1 day to 14 days	NDVI
Partially vegetated mudflats	Permanently dry raised mudflats beyond the influence of tidal or seasonal inundation except for extreme events	Non-seasonal extreme event (> 1 year)	Panchromatic brightness
Unvegetated mudflats	Ephemerally dry mudflats unable to support continuous vegetation cover	14 days to seasonal	Panchromatic brightness
Savannah woodland	Raised islands with sandstone substrate - enclosed by the floodplain but elevated above the temporal dynamics of surface water inundation	Permanently dry	NDVI
Creeks and drainage channels	Distributaries of the main river channel, permanently inundated	Permanently wet	Manual digitisation
Permanent water bodies	Areas of open water which remain inundated at all times	Permanently wet	NDPI
River Gambia/tributaries	Main river channel and its tributaries	Permanently wet	NDVI
Mid/riparian rice fields	Wamifaro/Bafaro types – tidally influenced	< 1 day to 14 days	NDVI
Peripheral rice fields	Bantafaro/Leofaro types - subject to pluvial inundation elevated above high tide levels	Rain-fed (Jun-Oct)	NDPI

Table 3
Total number of Landsat scenes available for each month.

Month	*n*	Season
JAN	7	Dry
FEB	11	Dry
MAR	12	Dry
APR	15	Dry
MAY	9	Dry
JUN	2	Wet
JUL	1	Wet
AUG	0	Wet
SEP	0	Wet
OCT	11	Wet
NOV	15	Dry
DEC	16	Dry
Total	99	

Table 4
Accuracy assessment class designations.

Original classes	Merged class	Class ID	Σ Test points
Halophytic vegetation Mid/riparian rice fields Peripheral rice fields	Halophytic vegetation	HV	600
Unvegetated ephemerally dry mudflats Partially vegetated permanently dry mudflats	Raised mudflats	MF	400
Permanent water Main channel/tributaries	Permanent water	PW	400
Mangrove	Mangrove	M	200
Savannah woodland	Savannah woodland	SW	200
Creeks/drainage channels	– Total	–	– 1800

2.5. Work package 2: geomorphological enhancement

DEM enhancement was based on the extent of vegetation cover under the assumption that the distribution of vegetation within the floodplain is dependent on semi-diurnal to bi-monthly differences in surface water extent. For example, areas classified as partially vegetated mudflats would remain dry at high tide and therefore exist at relatively high elevations compared to areas covered by halophytic vegetation that are frequently (diurnally) inundated, signifying areas of lower elevation (Table 2).

Geomorphological enhancement of the DEM involved six primary steps, outlined as follows:

1. The land cover classification was converted to polygons. Class boundaries were extracted as polylines from the resulting layer file in ArcMap 10.3. These polylines represented hydrological boundaries where a distinct change in elevation was expected based on the spatiotemporal analysis of morphological exposure (conceptually depicted in Fig. 5).
2. Land cover polygons were used to clip the SRTM DEM into discrete raster units based on the spatial distribution of hydrologically-influenced land cover.
3. Each water-based polyline was assigned an elevation value using daily minimum and maximum river stage data at Balingho (Fig. 1). The local vertical datum for the region is known as the Gambian Datum (GD) (Berry et al., 1985). The difference between GD as a local datum and mean sea level approximated by EGM96 (Earth Gravitational Model 1996: the geoid used as reference for orthometric height in SRTM) is unknown. For the purpose of this investigation, GD and EGM96 were presumed to be in agreement. River stage was converted to water surface elevation by summing stage height above chart datum (CD) at Balingho with height of CD above GD as follows:

$$\mathrm{CD}(0.731\ \mathrm{m}) + \mathrm{stage}(\mathrm{m}) = \text{water surface elevation (MSL)} \quad (3)$$

Average daily minimum and maximum stage in the dry season was used as vertical markers of low tide and high tide. Fortnightly high tide differences were used to establish spring tide stage (Table 5). The lower limit of the main channel/major tributaries was based on reach average depth of the study site (Albaret et al., 2004). The lower limit of bolons and drainage channels were based on reach average depth of bolon

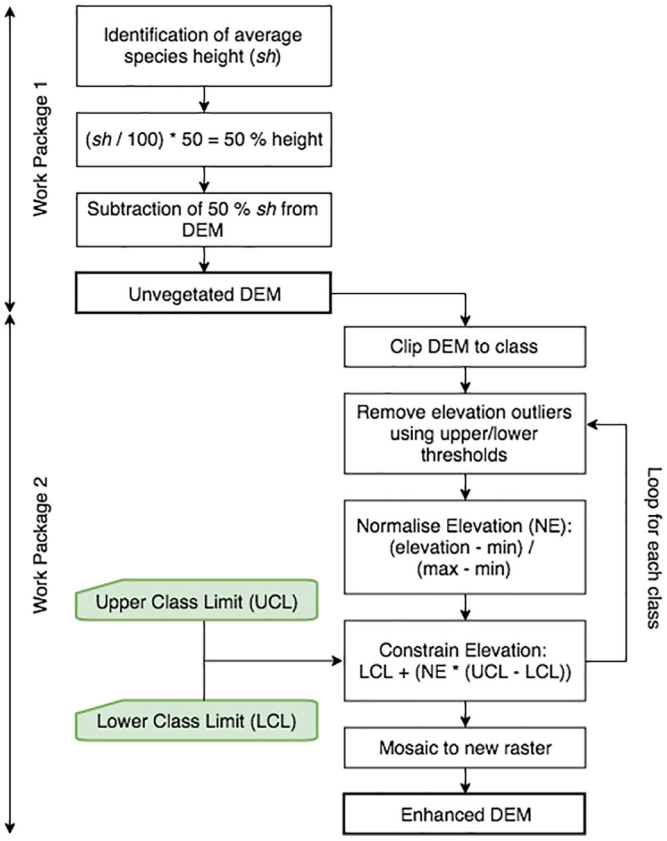

Fig. 4. Workflow for DEM enhancement.

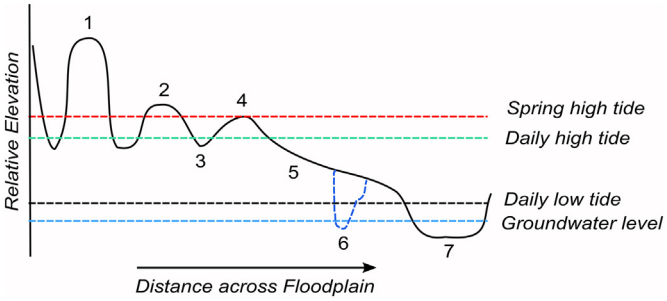

Fig. 5. Typical cross-section through floodplain morphology where: 1 = Raised island with sandstone substrate, 2 = raised alluvial mudflat (permanently dry), 3 = creek or drainage channel, 4 = raised alluvial mudflat (ephemerally dry), 5 = alluvial floodplain below daily/spring high tide level, 6 = permanent water body (groundwater-fed with or without tidal/seasonal inundation) and 7 = main river channel or tributary.

Table 5
Elevation thresholds– upper/lower limits in metres above sea level.

Class	Lower limit	Upper limit	Level type
Main channel/tributaries	−7.3	0.9	Low tide
Permanent waterbodies	−1.3	0.9	Low tide
Creeks/drainage channels	−1.3	0.9	Low tide
Mangrove	0.9	2.1	High tide
Halophytic vegetation	0.9	2.1	High tide
Mid/riparian rice fields	0.9	2.1	High tide
Unvegetated raised mudflats	2.1	2.4	Spring high tide
Partially vegetated raised mudflats	2.4	4	> Spring high tide
Peripheral rice fields	2.4	4	> Spring high tide
Savannah woodland	> 4		Non fluvial

features (Berry et al., 1985). The upper vertical limit of floodplain morphology (4 m above sea level) was based on average elevation (defined by the SRTM DEM) at the landward edge of alluvial sediments (defined by the land cover classification). Peripheral rice fields and unvegetated raised mudflats were considered to be within a similar elevation range, above tidal influence. Although mangrove and halophytic vegetation will contain some areas that are only inundated at spring high tide level (Table 2), the use of optical data limited the region to a holistic average high tide threshold (Table 5).

4. The elevation value of each waterline represented the upper/lower elevation boundary between two land cover classes (Table 5.). For example, halophytic vegetated areas should not exceed 2.1 m above sea level, and raised mudflats should equal or exceed, but never be below this value.

5. To constrain elevation across the land cover class between an upper and lower boundary, the following workflow was applied to each class individually using ArcMap 10.3:

a. Remove overlying vegetation cover.
b. Calculate the mean elevation value of the raster unit and determine outliers by selecting all the pixels of elevation > 3-sigma.

A 3-sigma outlier is defined as any value that is not found to be within 3 standard deviations of the mean. The subsequent z-score for each pixel was calculated as follows:

$$\text{Z-score} = (\text{value}/\text{mean})/\text{standard deviation}) \quad (4)$$

c. Modify outliers to equal the upper or lower elevation boundary of the class respective of whether the outlier was above the upper limit or below the lower limit for a class.
d. Normalise class elevation to lie on a scale between 0 and 1 by identifying the minimum and maximum elevation value as follows (where NE = Normalised Elevation):

$$NE = (\text{value} - \text{min})/(\text{max} - \text{min}) \quad (5)$$

e. Constrain elevation to lie between the stage-based upper class limit (UCL) and lower class limit (LCL) (see Table 5) as follows:

$$LCL + (NE * (UCL - LCL)) \quad (6)$$

6. Modified raster units were mosaicked to form an enhanced version of the SRTM DEM.

The resulting topographic profile of the enhanced DEM accentuated the height differences between hydrologically-driven land cover classes, and relative to this, supressed elevation variation across a class. Fig. 6 shows a conceptual cross-section of the floodplain. Note that in the original profile, the elevation differences of tidally-influenced swampland and desiccated, unvegetated mudflats is indistinguishable due to a high degree of random noise and interference from canopy height. In the corrected profile, vegetation is removed from swampland. The stripped profile is then constrained between an upper and lower stage boundary (in this example (not real values) between 3 and 5 m), at the zone of transition between classes (black lines). Accordingly, the elevation of swampland will never exceed the elevation of mudflats, dictated by the horizontal and vertical limits of daily high tide.

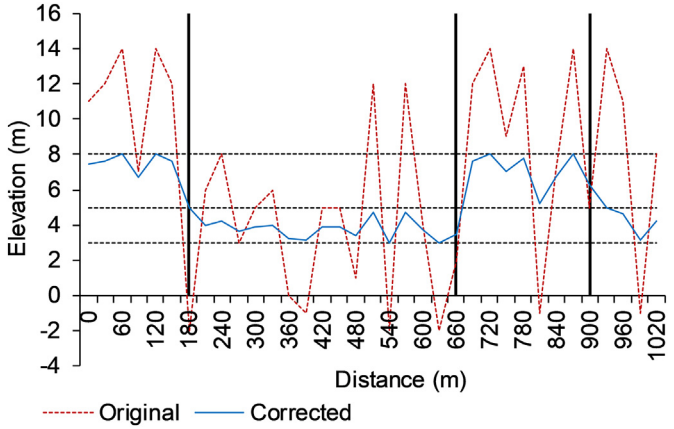

Fig. 6. Elevation enhancement across the floodplain (black lines represent the spatial limits of a morphological class; dotted black lines represent the upper and lower vertical height boundaries of halophytic swampland (3–5 m) and mudflats (5–8 m)).

2.6. Flood model parametrisation

The mechanistic flood model: LISFLOOD-FP (Bates et al., 2013) was used to assess the difference in floodwater extent between the original SRTM DEM (30 m) and enhanced DEM (30 m). The simulation was run under fixed conditions using a diffusive channel solver, with a downstream boundary condition representative of river stage at the downstream exit. A channel friction value of 0.02 and a floodplain friction value of 0.03 was established (respectively reflective of typical estuarine channel and vegetated floodplain conditions) (Chow, 1959). Channel bathymetry was burned into the DEM at a depth of 8 m, reflective of reach average depth across the study domain (Albaret et al., 2004). Downstream discharge data as well as upstream inflow within the tidal reach was not available for the area. Therefore, rather than modelling real flood events this study simulates theoretical flood events using a fixed discharge value of 1000 m^3/s. The value was applied firstly with a downstream boundary elevation of 1 msl (representing typical low tide conditions in the wet season) and increased in increments of 0.25 m to an elevation of 2.5 m (representing typical spring high tide conditions). In doing so, we are able to test the difference in flood extent predictions using i) the original DEM and ii) the enhanced DEM, to enable a direct comparison and assess the effectiveness of the enhancement approach outlined in this paper. Realistic flood extents are defined by the floodwater inundation contour limits determined from serial radar imagery (Sentinel 1).

3. Results

3.1. Flood frequency product – accuracy assessment

The land cover classification and subsequent temporal inundation map are shown in Figs. 7 and 8 respectively. An overall accuracy (OA) value of 93% was derived from the error matrix (Table 6) suggesting a strong level of agreement between established ground truth and predicted land cover. A Kappa coefficient value of 0.91 shows that the level

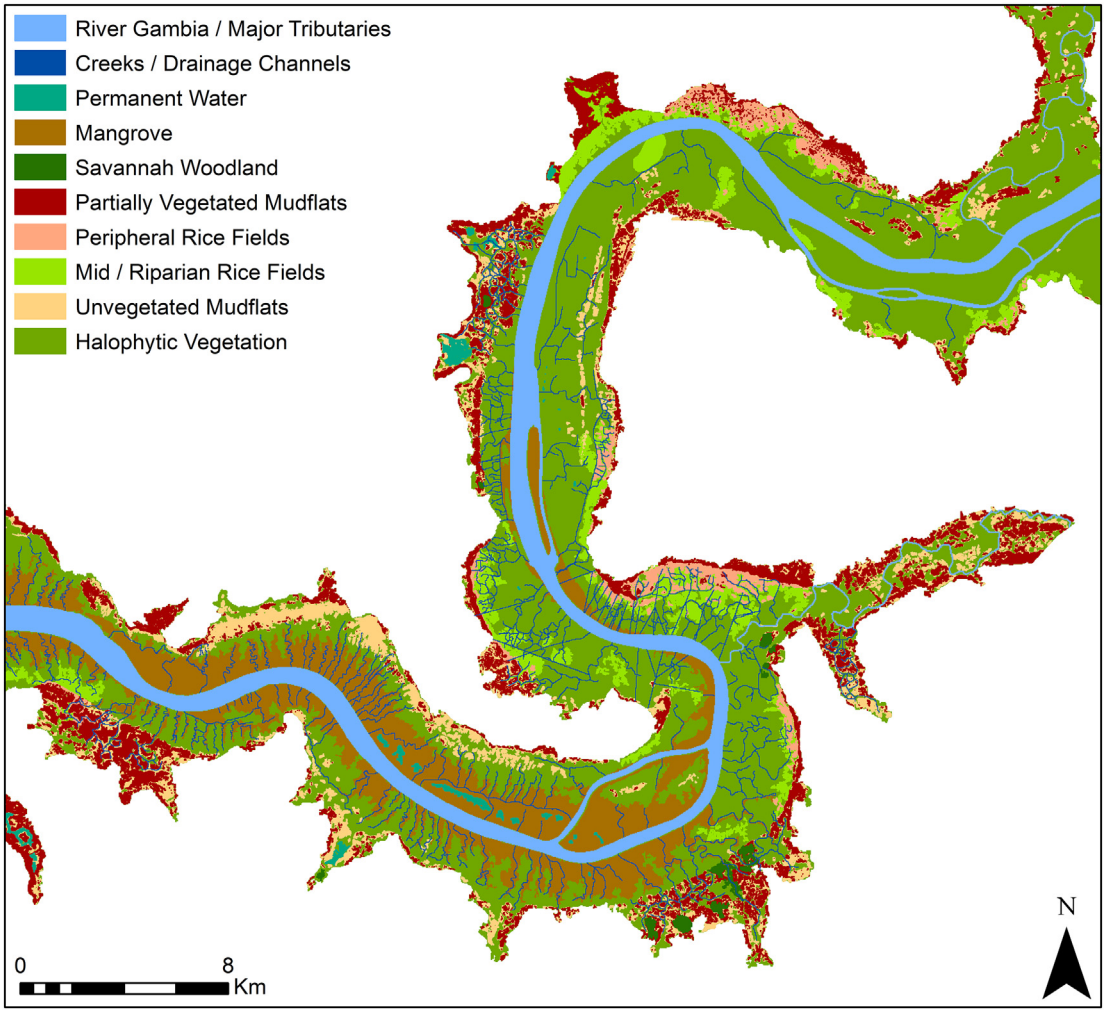

Fig. 7. Land cover classification based on the multi-temporal analysis of Landsat imagery (1986–2016).

of accuracy remained high following elimination of the proportion of agreement expected to occur by chance. As Table 7 shows, halophytic vegetation was the most dominant class, covering 58.9% of the study area. From a user-based perspective, confusion between halophytic vegetation and another class will have a proportionally greater effect on the overall accuracy of the map than confusion between other classes, covering a smaller area. To account for this, error was subsequently weighted by predicted area (km^2) per class. Weighted error reduced overall accuracy to 92%. The negligible change between the non-weighted and weighted matrix shows that misclassification within halophytic vegetation has a limited effect on the overall accuracy of the map. This is supported by a high producer and user accuracy of 91.4 and 89.6% respectively within the unweighted matrix. A Kappa coefficient value of 0.87 shows that when the areal dominance of halophytic vegetation is accounted for, the proportion of agreement expected to occur by chance remains low.

Confusion between most classes was minimal. In most cases, associated commission/omission error was found to be related to ground truth points located on the boundary between two classes. The confusion between mudflats and halophytic vegetation was due to the narrow nature of vegetated slacks between raised mudflats. Confusion was also identified between HV and PW which occurred due to the presence/absence of ephemeral aquatic vegetation between the reference and predicted products.

3.2. DEM enhancement

Fig. 9 compares the original SRTM DEM to the enhanced DEM for a section of the Gambian floodplain. Visual comparison between the two models demonstrated a reduction in noise and the subsequent delineation of floodplain morphology within the enhanced DEM. Separation was particularly discernible between raised mudflat features at the edge of the floodplain and low-lying swampland dominated by halophytic vegetation that characterises the majority of the floodplain (58.9%). The effect of vegetation removal is demonstrated towards the south of the region through the elimination of riparian and mid-stream mangrove forest.

Fig. 10 compares elevation values for a 1700 m cross-section along halophytic swampland. Normalisation of elevation preserves relative elevation across the morphological unit. However, overall elevation range has been reduced from 0 to 12 m to 1–2 m based on the known height of daily high tide. Fig. 11 shows elevation for a 6000 m cross-section within the floodplain demonstrating a clear reduction in height between the profiles of the original SRTM DEM and enhanced product, as a function of known inundation height. An apparent outlier of > 15 m occurs within the original DEM profile at ~3200 m across the floodplain (Fig. 11). This is indicative of the presence of tall mangrove trees present at the bank line. This feature is subsequently corrected within the enhanced DEM profile.

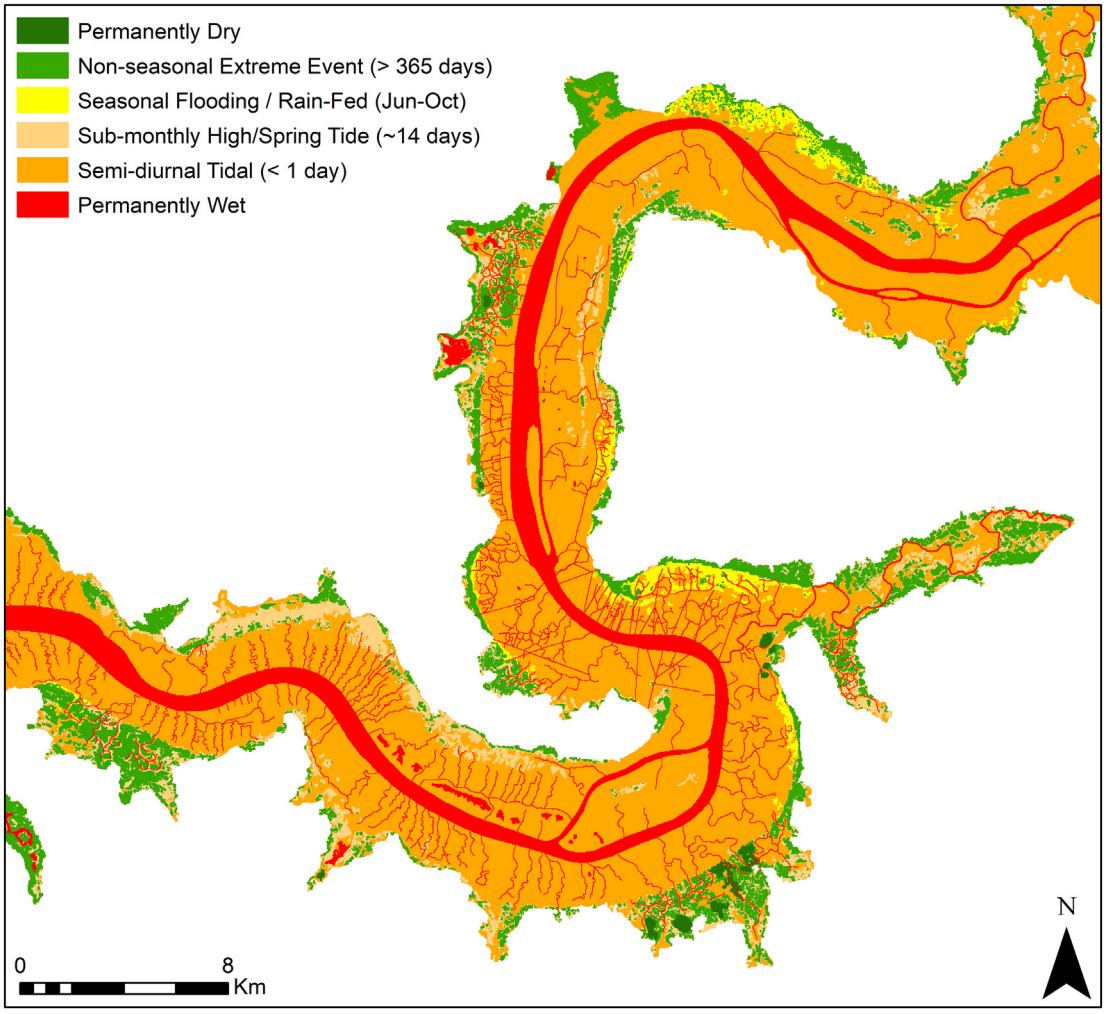

Fig. 8. Sub-annual spatio-temporal inundation map of the Gambian floodplain.

Table 6
Confusion matrix (N = 1800) where: HV = halophytic vegetation; MF = raised mudflats; SW = savannah woodland; M = mangrove; PW = permanent waterbodies; user/producer % = probability accuracy metrics regarding respective class commissions/omissions; OA = overall accuracy.

	HV	MF	SW	M	PW	User %
HV	563	49	5	8	3	89.6
MF	19	366	1	0	1	94.6
SW	11	5	178	0	0	91.8
M	9	0	0	187	2	94.4
PW	14	0	0	1	378	96.2
Producer %	91.4	87.1	96.7	95.4	98.4	1800
OA %	93					
Kappa	0.91					

3.3. Flood extent prediction

Fig. 12 shows fixed model outputs between 1.25 and 2 m river stage. Most regions predicted as being dry at 1.5–1.75 m align spatially with regions of mangrove forest cover (Fig. 12). This demonstrates that topographic variation across the inter-tidal zone is predominantly an artefact of vegetation height removal error. Fig. 13 compares the enhanced DEM flood model with the original DEM flood model. At both 2 m and 2.5 m, floodwater remained in-channel within the original DEM (Images C and D respectively). A tide height of 2.5 m should be sufficient to at least partially inundate regions of the floodplain associated with mangrove and halophytic vegetation. This shows that without modification, the SRTM DEM will vastly underestimate tidally influenced flood extent within the study reach. This underestimation is the result of: 1) continuous riparian mangrove growth at the bank line, forming an anomalous levee structure that subsequently prevents the channel from reaching bankfull conditions and 2) the absence of tidal distributaries (bolons) that route tidal water across the floodplain even when bankfull conditions of the main channel are not met.

Fig. 14 highlights the importance of the inclusion of negative and positive relief features within the floodplain in the routing of floodwater. As Image C shows, floodwater present at the floodplain periphery is routed via manually digitised bolons and through auxiliary pathways between raised mudflats. Comparison with a wet season aerial image (Image D) shows that peripheral regions are liable to flood during periods of high river stage. For context, Image A shows the absence of distinct geomorphological features within the original DEM.

4. Discussion

DEM enhancement techniques for medium-resolution SAR or optically-derived data include data hybridisation, water masking, stream burning, the implementation of fill/breaching algorithms and vegetation removal. These processes focus on improving the vertical accuracy of elevation data. However, there is limited focus on the reconciliation of small-scale complex topography within a DEM, in instances when vertical elevation error far exceeds the vertical range in floodplain morphology. This study presents an innovative method of DEM

Table 7
Predicted class area and % coverage. Weighted OA = overall accuracy weighted by predicted class area.

	Area (km^2)	% Area
HV	1144.45	58.9
MF	297.40	15.3
SW	8.18	0.4
M	257.86	13.3
PW	233.67	12.0
Total	1941.56	
Weighted OA %	92	
Kappa	0.87	

enhancement based on the multi-temporal classification of optical-based satellite imagery. Accuracy of the land cover classification and flood frequency derivative was 93% (92% weighted by area) with a kappa value of 0.91 (0.87 weighted by area). The classification was used to determine clear spatial boundaries in elevation change relative to tidal stage for the enhancement of a noise-filled DEM. The

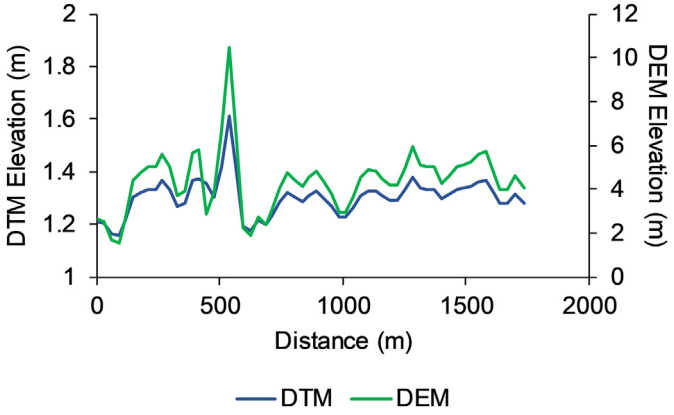

Fig. 10. Comparison of original DEM (DEM) and enhanced DEM (DTM) elevation across halophytic vegetation.

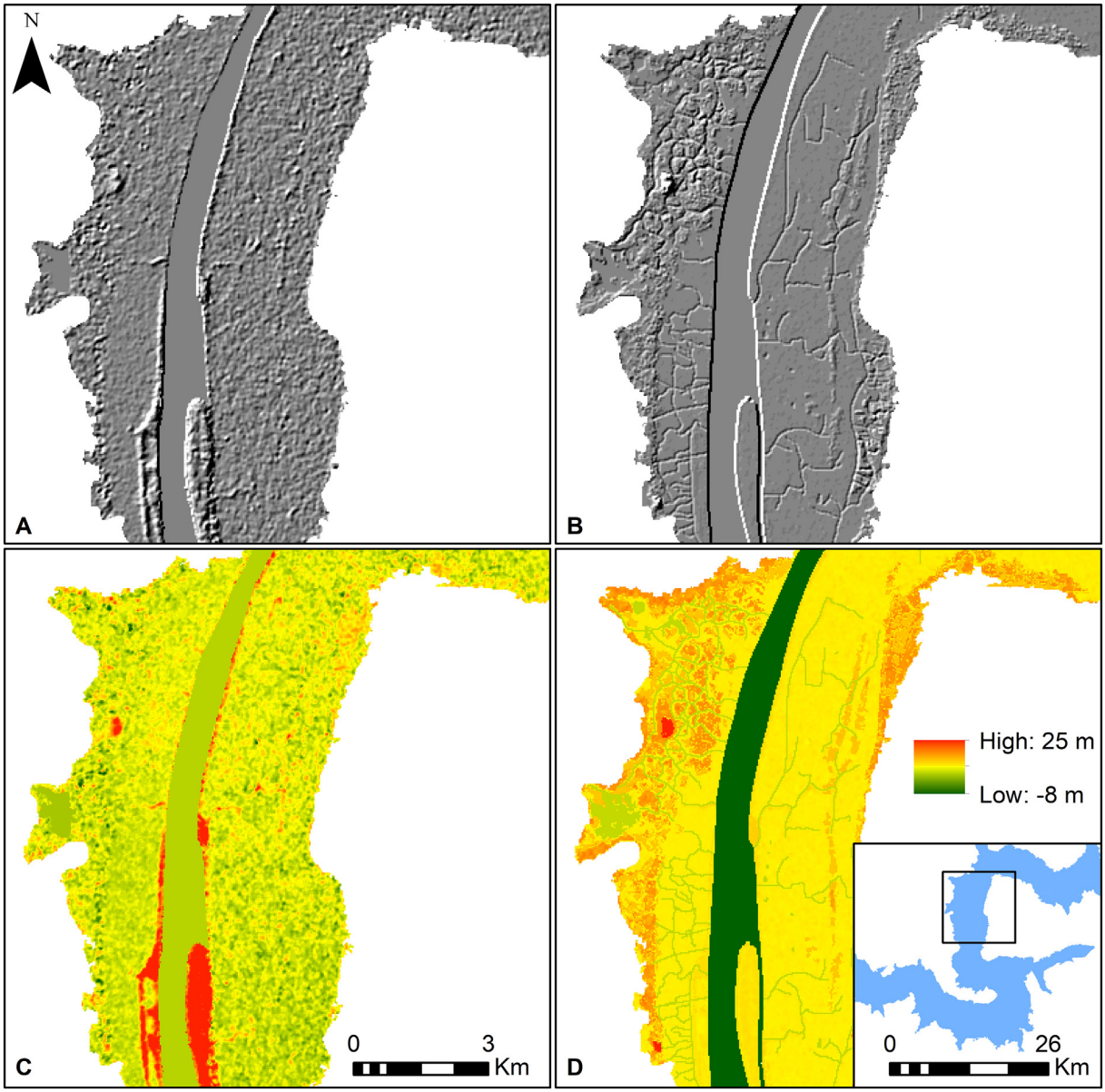

Fig. 9. Comparison of original DEM (C) and enhanced DEM (D). A and B shows corresponding hill-shade imagery for C and D respectively.

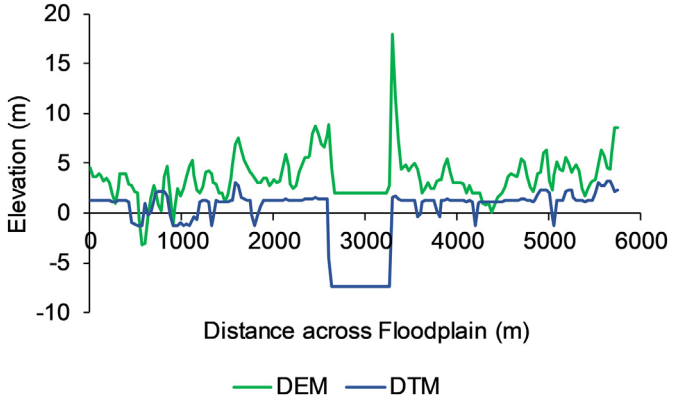

Fig. 11. Cross-section of original DEM (DEM) and enhanced DEM (DTM) floodplain topography.

comparison of flood extent prediction between the original and enhanced DEM suggests that, without modification, SRTM underestimates flood extent within the study region.

In densely vegetated floodplains such as this, the method relies predominantly on *a priori* knowledge of the spatial distribution of land cover in relation to surface water availability. Non-tidal floodplains associated with emergent vegetation may not exhibit the same degree of spatial heterogeneity in land cover. For example, the Barotse floodplain (Zambia) is covered almost exclusively in short, seasonally occurring grassland. As such, land cover transitions are of more limited use regarding geomorphological enhancement of underlying terrain. Furthermore, Non-tidal wetlands will typically have steeper valley gradients. The key assumption of this method is that water surface elevation varies negligibly across the reach, forming a near-planar surface. In steeper reaches, there will be a greater difference between water surface elevation at the point of inflow and the point of outflow. As such, in order to use downstream stage as an elevation threshold, an additional adjustment step in DEM enhancement would have to be implemented that weights the elevation value of a pixel within the same geomorphological unit by distance upstream (e.g. Merwade, 2009).

However, the geomorphological enhancement technique is expected to be relevant to other low-gradient, tidally-influenced tropical regions where vegetation cover is heterogeneously distributed and predominantly a function of topographically-controlled surface water inundation. Furthermore, the near-global availability of medium-resolution products such as SRTM allows this technique to represent a tractable methodology for application to other data sparse environments.

Regarding application to both tidal and non-tidal regions, this study highlights the importance of resolving complex topography for the purpose of hydraulic modelling. As Fig. 14 suggests, the routing of floodwater to the floodplain periphery is dependent on tidal distributaries known as bolons rather than direct inundation from the main channel. In a fixed hydraulic simulation such as this (where the focus is on predicting maximum extent of floodwater under steady state conditions), the absence of such features impacts only the accuracy of flood extent prediction. However, in a dynamic simulation, omission of these key routing features may also affect water storage representation, mechanisms of floodplain filling/dewatering and ultimately, the prediction of flood wave travel time (e.g. Horritt and Bates, 2001; Wilson et al., 2007). Furthermore, as previously noted, the ability to facilitate hydrological connectivity across a floodplain depends on the chosen DEM resolution relative to study domain extent and computational performance of the flood model. The size of Gambia study reach was chosen specifically to allow the representation of small-scale fluvial features. However, it is recognised that such an approach may not yet be re-scalable in relation to larger reaches of $> 10{,}000\ km^2$.

4.1. Practical applications in hydraulic modelling

A key advantage of the enhanced DEM for the Gambia study site is that it is now appropriate for use in hydraulic flood modelling. Potential applications include assessing the effect of future damming of the River Gambia further upstream on water availability and salinity concentration within the study area (Degeorges and Reilly, 2007). Accordingly, the short-term and long-term impacts on agriculture and ecology can be evaluated. A hydrologically accurate surface profile has far-reaching impacts on the ability of water resource managers in data sparse regions (such as sub-Saharan Africa) to model floodwater both as a hazard and as a resource in terms of delivery of seasonal water for use in irrigated agricultural schemes (e.g., Carney, 1998a, 1998b; Baeza et al., 2013). Future discharge predictions can be used in conjunction with the enhanced DEM to assess changes in flood risk in relation to climate change scenarios (e.g. Ardoin-Bardin et al., 2009).

Improvements in flood prediction accuracy through DEM enhancement will also be of benefit to public health managers (Cole et al., 2014; Hagen and Lu, 2011). For instance, vulnerable communities living within the floodplains of large rivers become periodically cut-off from important resources such as the timely delivery of HIV drugs or assistance in child birth: factors that represent a key challenge to public health managers in regions like the Barotseland floodplain of the Zambezi River, Western Zambia (Cai et al., 2016). By using flood models to provide real-time maps of water inundation, public health managers can make decisions on how best to reach people in need: overland motor vehicles or by boat.

An additional public health benefit made possible through accurate floodwater inundation mapping is their use in mosquito-borne disease control campaigns. Specifically, an important strategy for controlling the transmission of diseases like malaria is the use of larvicide in waterbodies used by mosquitoes for oviposition and larval development (Hardy et al., 2013; Majambere et al., 2008 and 2010). However, the success of this approach hinges on our ability to map waterbodies over large areas (Majambere et al., 2008 and 2010). By using the methods presented in this paper to enhance freely available DEMs, the potential for providing timely and accurate maps of potential mosquito aquatic habitats in floodplains becomes a reality.

4.2. Study limitations

The majority of change in surface water extent within the study region is a function of sub-daily tide rather than inter-seasonal change. At day-scale (based on stage readings between 2015 and 2016), the daily range in tidal stage exceeds seasonal range (i.e. the difference in high tide stage in the wet season and dry season is negligible - Fig. 2). Therefore, the study was limited in part by the acquisition period between available data. The temporal frequency between optical scenes ($\geq$14 days) did not allow for semi-diurnal tidal dynamics to be quantified directly. As a result, tidal limits were inferred from the extent of saline-tolerant vegetation (Yanlong et al., 2011). Furthermore, stage readings used to define the upper and lower limits of hydrological boundaries were based on a relatively short measurement period of 2 years (2015–2016) and therefore may not have accounted for the vertical limits of inundation events that exceed this return period. The possibility of an offset between river stage (vertically referenced to the Gambian Datum (GD)) and orthometric elevation of the SRTM DEM (relative to EGM96) cannot be discounted.

Freely-available archived SAR data (e.g. Sentinel 1) has the potential to improve DEM enhancement as inundation dynamics can be reconciled directly underneath vegetation cover. However, the temporal frequency of archived image acquisitions is also typically > 1 day. Furthermore, there was no access to high-resolution stage data timed to the nearest hour of image acquisition, as a remedial dataset for tide level assessment. As such, it was not possible to categorise available imagery by low, high, neap or spring tide stage based on the time stamp

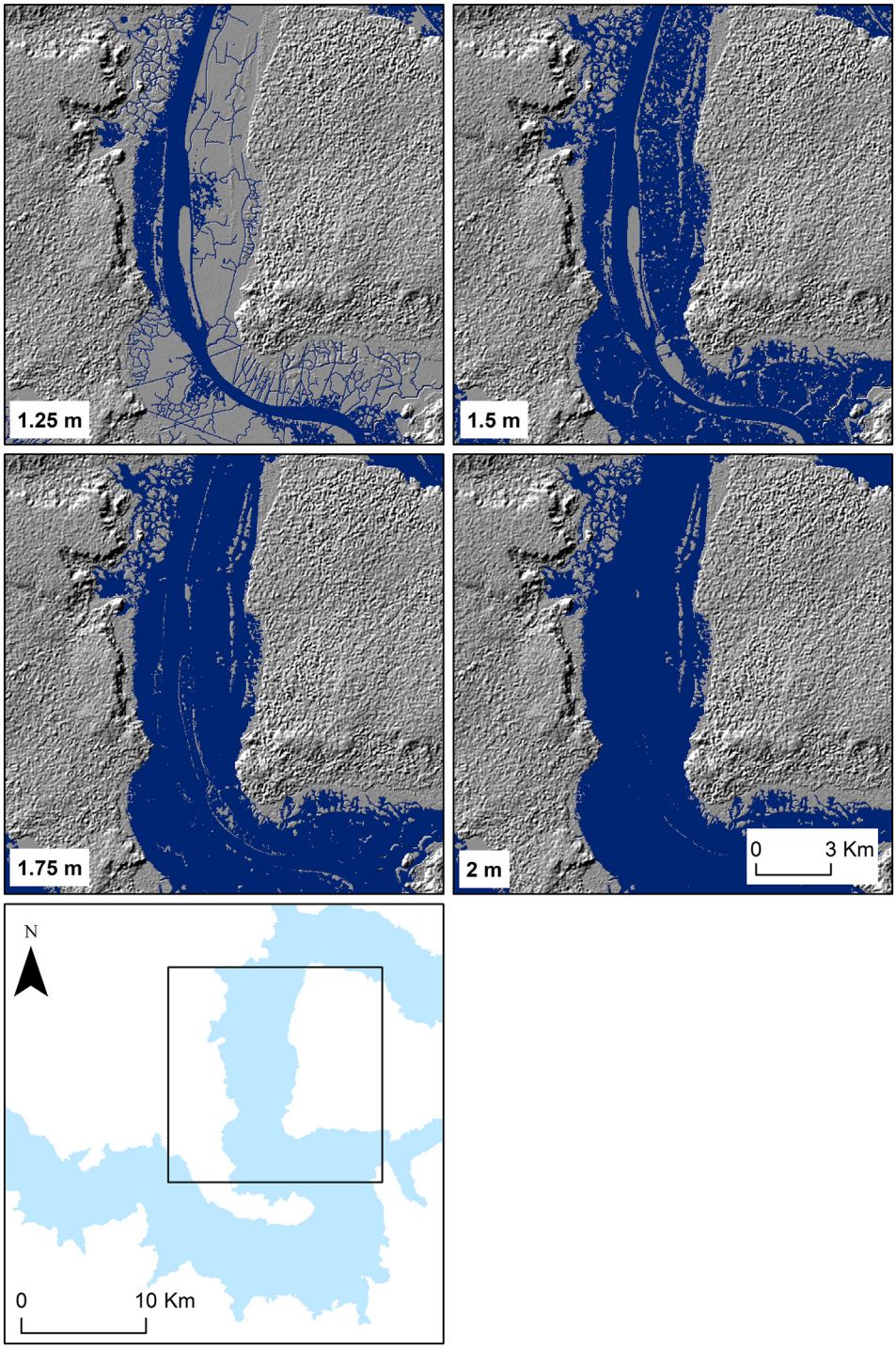

Fig. 12. Flood extent prediction with stage at the downstream boundary of 1.25–2 m above sea level.

of image acquisition. As previously identified, C-band radar also offers limited capabilities of water detection under closed canopy mangrove, suggesting that the use of SAR data would not be advantageous over optical data within such regions. Therefore, from a remote sensing perspective, the extent of tidally-influenced vegetation is the most robust indicator of the maximum extent of tidal flooding within a data sparse region such as this. The use of archived Landsat imagery was considered to be suitable for the classification of land cover and water extent in this regard.

Vegetation removal was based on a rudimentary estimate of average species height. For example, mangrove canopy removal was parameterised using average known height of the species *Rhizophora* sp. (20 m). However, *Rhizophora* sp. forms mixed stands with *Avicennia* sp. between the average daily high and spring tide zone. *Avicennia* sp. has a much shorter average height of ≤7 m (Twilley, 1985). This suggests that DEM enhancement could be improved through a more detailed partitioning of canopy height, based on species variation. Availability of GCPs or a high-resolution terrain model in conjunction with either X-band SAR (e.g. Rabus et al., 2003), optical-stereo or laser altimetry-derived canopy height estimation (e.g. ICESat) would also allow a more robust estimate of the canopy penetration potential of the C-band derived SRTM DEM. As suggested by the flood model (Fig. 12), regions

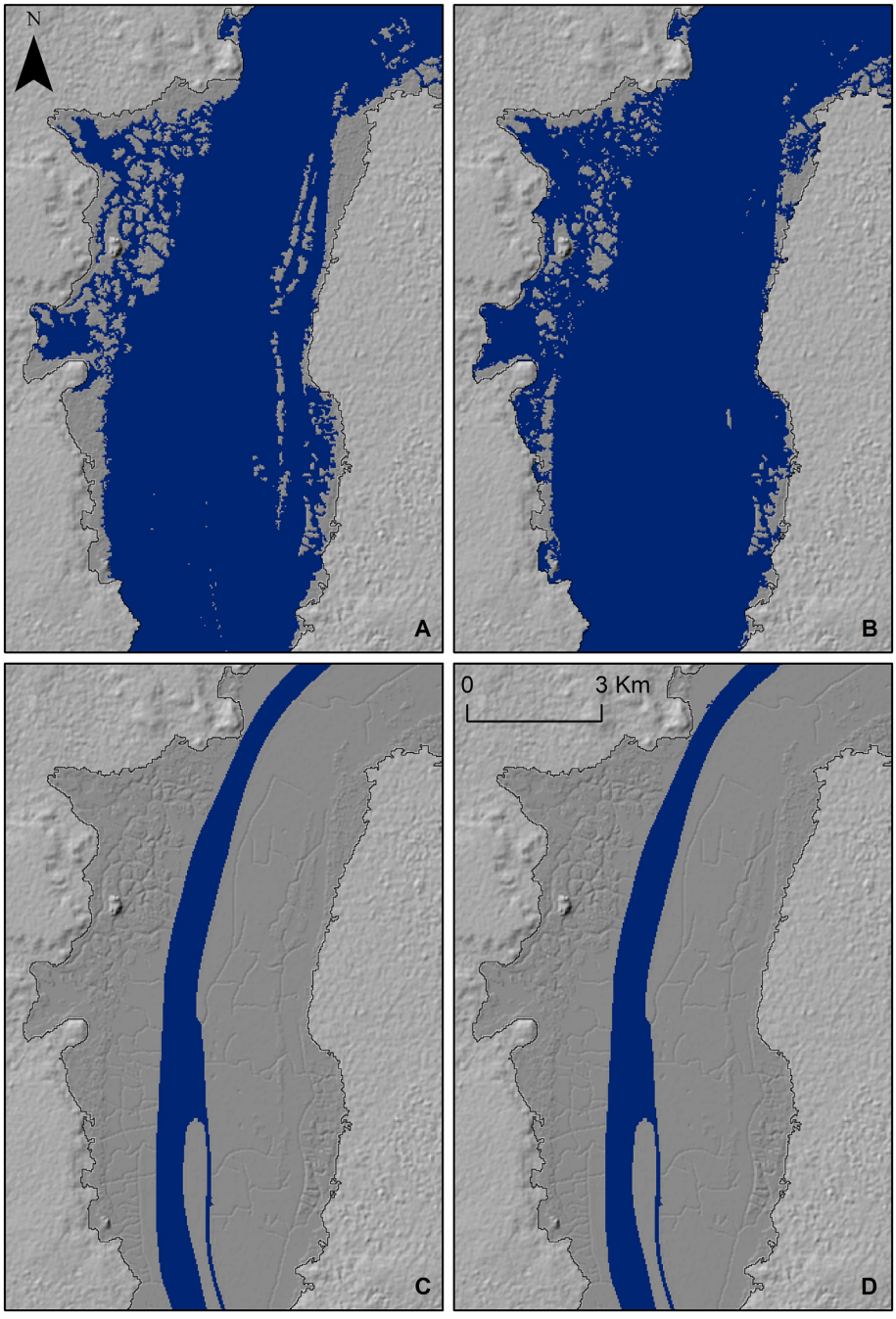

Fig. 13. Predicted flood extent where: A = 2 m over enhanced DEM; B 2.5 m over enhanced DEM; C = 2 m over original DEM and D = 2.5 m over original DEM. Flood predictions overlay hill shade imagery (dark grey = floodplain; light grey = outside of floodplain). Black line = extent of alluvial sediments.

covered by mangrove were associated with an overestimation of elevation, thereby indicating that 50% was an exaggeration of the canopy penetration potential of SRTM in comparison to halophytic vegetation. Future study regarding DEM enhancement within data sparse regions should consider the use of vegetation height removal as a calibration parameter for flood model performance.

However, geomorphological enhancement effectively mutes vegetation removal height error and random noise by normalising the variation between strict geomorphological boundaries. Relative vertical accuracy *within* a geomorphological unit will not show as much of an improvement as relative vertical accuracy *between* geomorphological units within the enhanced DEM. Simply put, the inter-tidal region containing halophytic vegetation and mangrove is still noisy following vegetation removal. However, this noise is supressed by accentuating the presence of raised mudflats and rain-fed peripheral rice fields on higher ground as positive relief formations; and bolons, drainage channels, and permanent pools as negative relief formations within the floodplain. A further improvement could be made to the SRTM DEM by performing coarse pixel aggregation prior to implementation of the enhancement technique (e.g. Wilson et al., 2007). DEM resolution could subsequently be resampled to its original resolution. In doing so, shortwave error (pixel-to-pixel) would be minimised, but optimal grid spacing for the representation of small-scale topographic features through geomorphological enhancement would be preserved.

5. Conclusion

This study has presented a new technique for the enhancement of

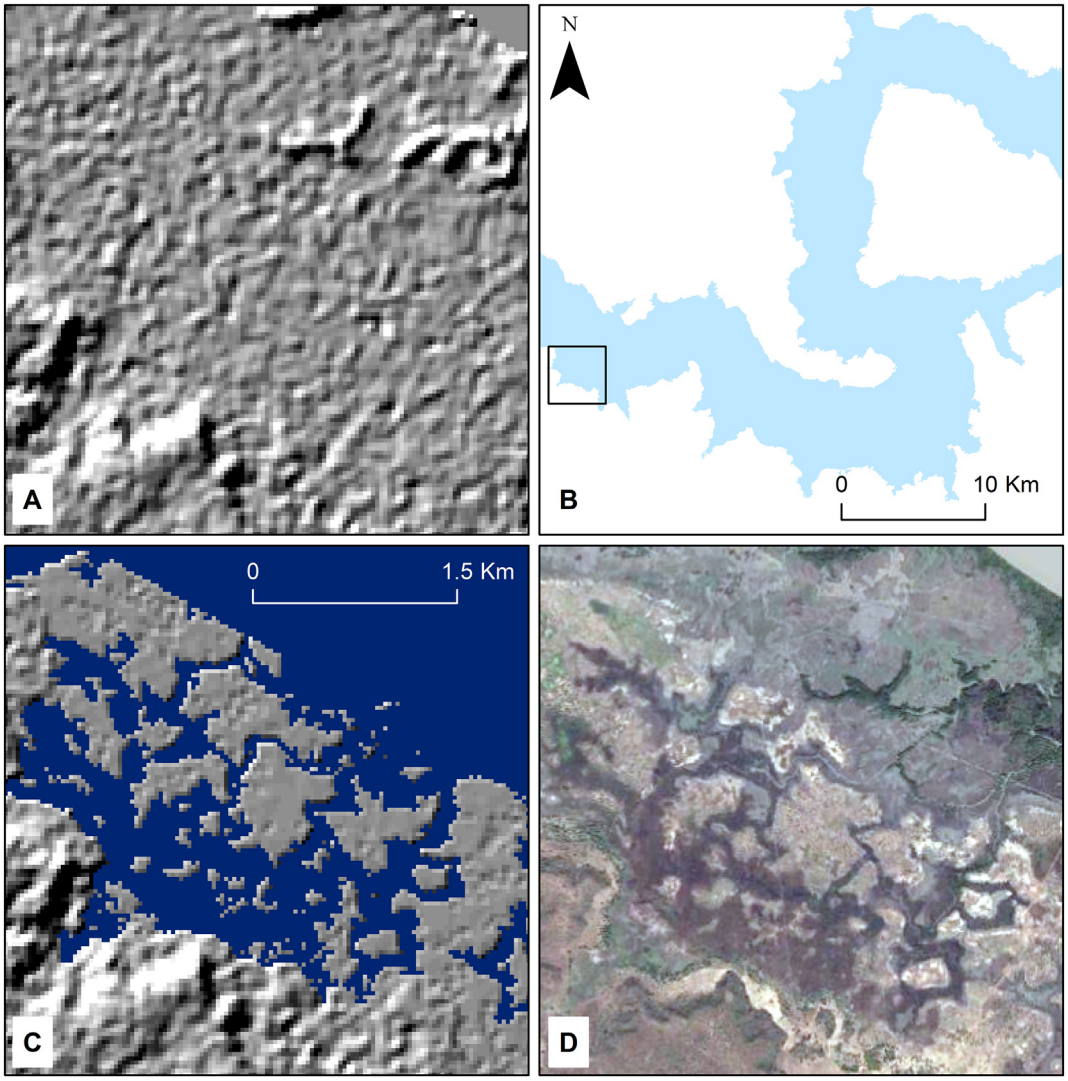

Fig. 14. Demonstrating an improvement in flood routing across the Gambia floodplain. Image A = Hill shade image of the original DEM; Image B = Location of Images A, C and D within the floodplain (black box); Image C = Inundation of the floodplain periphery via bolons following geomorphological enhancement of the DEM; Image D = True colour aerial image (source: Google Earth) dated October 2014, depicting wet season flood extent.

medium-resolution DEMs. Products such as the InSAR derived SRTM DEM are widely applicable in data sparse regions as non-proprietary, globally available datasets. However, the vertical error margin of these DEMs will typically exceed the vertical range in floodplain topography and flood wave amplitude, even within large-scale river systems. Without modification, these products are not suitable for use within mechanistic flood model applications, designed to simulate topographically-controlled overbank flow across a floodplain. The DEM enhancement technique, presented therein, focuses on the spatiotemporal frequency of surface water distribution for topographic correction. The method renders medium-resolution DEMs as fit-for-purpose within 2D flood model applications, in regions where accurate flood assessment is precluded by a lack of ground data or high-resolution Earth Observation data. The method is applicable to regions in which the spatiotemporal dynamics of surface water availability and associated distribution of vegetation is controlled predominantly by semi-diurnal to monthly variations in river stage, as a function of tide. Further testing is required to determine whether the method will be applicable to non-tidal regions with steeper valley gradients and greater homogeneity in land cover. Applicability of the technique also depends on the desired domain extent of available DEM data: The rectification of small-scale complex morphology within a DEM is key to a robust estimation of flood extent, floodplain storage capacity and flood wave travel time. However, computational efficiency of simulated flow may require a compromise between effective topographic representation and optimal DEM resolution.

Acknowledgements

The authors would like to thank the four anonymous reviewers for their helpful and constructive feedback that has helped strengthen this paper. We are also grateful to ESA for the provision of the ALOS PRISM imagery. This research was supported by the Doctoral Career Development Scholarship at Aberystwyth University (UK) and the Natural Environment Research Council (NERC) (NE/P013481/1). The authors would also like to thank Silas Majambere and Chris Thomas for their advice and support.

References

Abrams, M., 2016. Aster global dem version 3, and new aster water body dataset. In: International Archives of the Photogrammetry, Remote Sensing and Spatial Information Sciences - ISPRS Archives, 41(July), pp. 107–110. https://doi.org/10.5194/isprsarchives-XLI-B4-107-2016.

Albaret, J.J., Simier, M., Darboe, F.S., Ecoutin, J.M., Raffray, J., de Morais, L.T., 2004.

Fish diversity and distribution in the Gambia Estuary, West Africa, in relation to environmental variables. Aquat. Living Resour. 17 (1), 35–46. https://doi.org/10.1051/alr.

Amarnath, G., Umer, Y.M., Alahacoon, N., Inada, Y., 2015. Modelling the flood-risk extent using LISFLOOD-FP in a complex watershed: case study of Mundeni Aru River Basin, Sri Lanka. In: IAHS-AISH Proceedings and Reports. 370. pp. 131–138. https://doi.org/10.5194/piahs-370-131-2015.

Ardoin-Bardin, S., Dezetter, A., Servat, E., Paturel, J.E., Mahé, G., Niel, H., Dieulin, C., 2009. Using general circulation model outputs to assess impacts of climate change on runoff for large hydrological catchments in West Africa. Hydrol. Sci. J. 54 (April 2015), 77–89. https://doi.org/10.1623/hysj.54.1.77.

Baeza, A., Bouma, M.J., Dhiman, R.C., Baskerville, E.B., Ceccato, P., Yadav, R.S., Pascual, M., 2013. Long-lasting transition toward sustainable elimination of desert malaria under irrigation development. Proc. Natl. Acad. Sci. 110 (37), 15157–15162. https://doi.org/10.1073/pnas.1305728110.

Bates, P.D., 2012. Integrating remote sensing data with flood inundation models: how far have we got? Hydrol. Process. 26, 2515–2521.

Bates, P., Trigg, M., Neal, J., Dabrowa, A., 2013. 'LISFLOOD-FP User Manual', (November). pp. 1–49.

Baugh, C.A., Bates, P.D., Schumann, G., Trigg, M.A., 2013. SRTM vegetation removal and hydrodynamic modeling accuracy. Water Resour. Res. 49 (9), 5276–5289. https://doi.org/10.1002/wrcr.20412.

Berry, D.T., Moll, R.A., Krausse, G.L., 1985. Physical and Chemical Environment of the Gam bia River, West Africa. pp. 1983–1984.

Biancamaria, S., Bates, P.D., Boone, A., Mognard, N.M., 2009. Large-scale coupled hydrologic and hydraulic modelling of the Ob river in Siberia. J. Hydrol. 379 (1–2), 136–150. https://doi.org/10.1016/j.jhydrol.2009.09.054. Elsevier B.V.

Bøgh, C., Clarke, S.E., Jawara, M., Thomas, C.J., Lindsay, S.W., 2003. Localized breeding of the *Anopheles gambiae* complex (Diptera: Culicidae) along the River Gambia, West Africa. Bull. Entomol. Res. 93 (4), 279–287. https://doi.org/10.1079/BER2003239. Aberystwyth University.

Bøgh, C., Lindsay, S.W., Clarke, S.E., Dean, A., Jawara, M., Pinder, M., Thomas, C.J., 2007. High spatial resolution mapping of malaria transmission risk in the Gambia, west Africa, using LANDSAT TM satellite imagery. Am. J. Trop. Med. Hyg. 76 (5), 875–881. Available at. http://www.ncbi.nlm.nih.gov/pubmed/17488908.

Cai, X., Haile, A.T., Magidi, J., Mapedza, E., Nhamo, L., 2016. Living with floods - household perception and satellite observations in the Barotse floodplain, Zambia. Phys. Chem. Earth 1–9. https://doi.org/10.1016/j.pce.2016.10.011. Elsevier Ltd.

Carney, J.A., 1998a. Rice cultivation and Gambian women. In: Gender Analysis and Reform of Irrigation Management: Concepts, Cases, and Gaps in Knowledge: Proceedings of the Workshop on Gender and Water. International Water Management Institute, Habarana, Sri Lanka, pp. 151–169.

Carney, J.A., 1998b. Women's land rights in Gambian irrigated rice schemes: constraints and opportunities. Agric. Hum. Values 15 (4), 325–336. https://doi.org/10.1023/A:1007580801416.

Chow, V.T., 1959. Open-channel Hydraulics. McGraw-Hill, New York, USA.

Coe, M.T., Costa, M.H., Howard, E.A., 2008. Simulating the surface waters of the Amazon River basin: impacts of new river geomorphic and flow parameterizations. Hydrol. Process. 22, 2542–2553.

Cole, S., van Koppe, B., Puskur, R., Estrada, N., DeClerk, F., Badu-Forson, J., Remans, R., Mapedza, E., Longley, C., Muyaule, C., Zulu, F., 2014. Collaborative effort to operatioalize the gender transformative approach in the Barotse Floodplain. Available at: http://aas.cgiar.org/sites/default/files/publications/files/AAS-2014-38.pdf.

da Paz, A.R., Collischonn, W., Tucci, C.E.M., Padovani, C.R., 2011. Large-scale modelling of channel flow and floodplain inundation dynamics and its application to the Pantanal (Brazil). Hydrol. Process. 25 (9), 1498–1516. https://doi.org/10.1002/hyp.7926.

Day, G., Dietrich, W.E., Rowland, J.C., Marshall, A., 2008. The depositional web on the floodplain of the Fly River, Papua New Guinea. J. Geophys. Res. Earth Surf. 113 (1), 1–19. https://doi.org/10.1029/2006JF000622.

de Carvalho Junior, O.A., Guimaraes, R.F., Montgomery, D.R., Gillespie, A.R., Gomes, R.A.T., de S. Martins, E., Silva, N.C., 2014. Karst depression detection using ASTER, ALOS/PRISM and SRTM-derived digital elevation models in the Bambuí group, Brazil. Remote Sens. 6 (1), 330–351. https://doi.org/10.3390/rs6010330.

Degeorges, A., Reilly, B.K., 2007. Eco-politics of dams on the Gambia river. Int. J. Water Resour. Dev. 23 (4), 641–657. https://doi.org/10.1080/07900620701488588.

Fillinger, U., Sombroek, H., Majambere, S., van Loon, E., Takken, W., Lindsay, S.W., 2009. Identifying the most productive breeding sites for malaria mosquitoes in the Gambia. Malar. J. 8, 62. https://doi.org/10.1186/1475-2875-8-62.

Gorokhovich, Y., Voustianiouk, a, 2006. Accuracy assessment of the processed SRTM-based elevation data by CGIAR using field data from USA and Thailand and its relation to the terrain characteristics. Remote Sens. Environ. 104 (4), 409–415. https://doi.org/10.1016/j.rse.2006.05.012.

Guillard, J., Albaret, J.-J., Simier, M., Sow, I., Raffray, J., Tito De Morais, L., 2004. Spatio-temporal variability of fish assemblages in the Gambia Estuary (West Africa) observed by two vertical hydroacoustic methods: moored and mobile sampling. Aquat. Living Resour. 17 (1), 47–55. https://doi.org/10.1051/alr:2004005.

Hagen, E., Lu, X.X., 2011. Let us create flood hazard maps for developing countries. Nat. Hazards 58 (3), 841–843. https://doi.org/10.1007/s11069-011-9750-7.

Hardy, A.J., Gamarra, J.G.P., Cross, D.E., Macklin, M.G., Smith, M.W., Kihonda, J., Killeen, G.F., Ling'ala, G.N., Thomas, C.J., 2013. Habitat hydrology and geomorphology control the distribution of malaria vector larvae in rural Africa. PLoS One 8 (12), 1–13. https://doi.org/10.1371/journal.pone.0081931.

Hay, S.I., Snow, R.W., Rogers, D.J., 1998. Predicting malaria seasons in Kenya using multitemporal meteorological satellite sensor data. Trans. R. Soc. Trop. Med. Hyg. 92 (1), 12–20. https://doi.org/10.1016/S0035-9203(98)90936-1.

Hellweger, F., 1997. AGREE - DEM surface reconditioning system. Available at: http://www.ce.utexas.edu/prof/maidment/gishydro/ferdi/research/agree/agree.html, Accessed date: 22 June 2017.

Henderson, F.M., Lewis, A.J., 2008. Radar detection of wetland ecosystems: a review. Int. J. Remote Sens. 29 (20), 5809–5835. https://doi.org/10.1080/01431160801958405.

Hess, L.L., Melack, J.M., Novo, E.M.L.M., Barbosa, C.C.F., Gastil, M., 2003. Dual-season mapping of wetland inundation and vegetation for the central Amazon basin. Remote Sens. Environ. 87 (4), 404–428. https://doi.org/10.1016/j.rse.2003.04.001.

Horritt, M.S., Bates, P.D., 2001. Effects of spatial resolution on a raster based model of flood flow. J. Hydrol. 253.

Horritt, M.S., Mason, D.C., Cobby, D.M., Davenport, I.J., Bates, P.D., 2003. Waterline mapping in flooded vegetation from airborne SAR imagery. Remote Sens. Environ. 85 (3), 271–281. https://doi.org/10.1016/S0034-4257(03)00006-3.

Jenson, S.K., Domingue, J.O., 1988. Extracting topographic structure from digital elevation data for geographic information system analysis. Photogramm. Eng. Remote. Sens. 54 (11), 1593–1600 (doi:0099-1112/88/5411-1593$02.25/0).

Kasischke, E.S., Bourgeau-Chavez, L.L., 1997. Monitoring South Florida wetlands using ERS-1 SAR imagery. Photogramm. Eng. Remote. Sens. 63 (3), 281–291. Available at. http://www.asprs.org/publications/pers/97journal/march/1997_mar_281-291.pdf.

Kiage, L.M., Walker, N.D., Balasubramanian, S., Babin, A., Barras, J., 2005. Applications of Radarsat-1 synthetic aperture radar imagery to assess hurricane-related flooding of coastal Louisiana. Int. J. Remote Sens. 26 (24), 5359–5380. https://doi.org/10.1080/01431160500442438.

Komi, K., Neal, J., Trigg, M.A., Diekkrüger, B., 2017. Modelling of flood hazard extent in data sparse areas: a case study of the Oti River basin, West Africa. J. Hydrol. Reg. Stud. 10, 122–132. https://doi.org/10.1016/j.ejrh.2017.03.001. Elsevier B.V.

Kreiselmeier, J., 2015. Development of a Flood Model Based on Globally-available Satellite Data for the Papaloapan River, Mexico.

Lefsky, M.A., 2010. A global forest canopy height map from the moderate resolution imaging spectroradiometer and the geoscience laser altimeter system. Geophys. Res. Lett. 37 (L15401), 1–5. https://doi.org/10.1029/2010GL043622.

Lehner, B., Verdin, K., Jarvis, A., 2008. New global hydrography derived from spaceborne elevation data. Eos 89 (10), 93–94. https://doi.org/10.1029/2008EO100001.

Leveque, C., 1995. River and stream ecosystems of Northwestern Africa. In: Cushing, C.E., Cummins, K.W., Minshall, G.W. (Eds.), River and Streams Ecosystems. Elsevier, New York, pp. 519–536.

Lewin, J., Ashworth, P.J., 2014. The negative relief of large river floodplains. Earth Sci. Rev. 129, 1–23. https://doi.org/10.1016/j.earscirev.2013.10.014.

Lewis, M., Bates, P., Horsburgh, K., Neal, J., Schumann, G., 2013. A storm surge inundation model of the northern bay of Bengal using publicly available data. Q. J. R. Meteorol. Soc. 139 (671), 358–369. https://doi.org/10.1002/qj.2040.

Lindsay, J.B., 2016. The practice of DEM stream burning revisited. Earth Surf. Process. Landf. 41 (5), 658–668. https://doi.org/10.1002/esp.3888.

Lindsay, J.B., Creed, I.F., 2005a. Removal of artifact depressions from digital elevation models: towards a minimum impact approach. Hydrol. Process. 19 (16), 3113–3126. https://doi.org/10.1002/hyp.5835.

Lindsay, J.B., Creed, I.F., 2005b. Sensitivity of digital landscapes to artifact depressions in remotely-sensed DEMs. Photogramm. Eng. Remote. Sens. 71 (9), 1029–1036. https://doi.org/10.14358/PERS.71.9.1029.

Long, S., Fatoyinbo, T.E., Policelli, F., 2014. Flood extent mapping for Namibia using change detection and thresholding with SAR. Environ. Res. Lett. 9 (3). https://doi.org/10.1088/1748-9326/9/3/035002.

Louca, V., Lindsay, S.W., Majambere, S., Lucas, M.C., 2008. Fish community characteristics of the lower Gambia River floodplains: a study in the last major undisturbed West African river. Freshw. Biol. 54 (2), 254–271. https://doi.org/10.1111/j.1365-2427.2008.02105.x.

Lu, Z., Kwoun, O., 2009. Interferometric Synthetic Aperture Radar (InSAR) study of coastal wetlands over Southeastern Louisiana. In: Remote Sensing of Coastal Environments, pp. 25–60.

Majambere, S., Fillinger, U., Sayer, D.R., Green, C., Lindsay, S.W., 2008. Spatial distribution of mosquito larvae and the potential for targeted larval control in the Gambia. Am. J. Trop. Med. Hyg. 79 (1), 19–27 (doi:79/1/19 [pii]).

Majambere, S., Pinder, M., Fillinger, U., Ameh, D., Conway, D.J., Green, C., Jeffries, D., Jawara, M., Milligan, P.J., Hutchinson, R., Lindsay, S.W., 2010. Is mosquito larval source management appropriate for reducing malaria in areas of extensive flooding in the Gambia? A cross-over intervention trial. Am. J. Trop. Med. Hyg. 82 (2), 176–184. https://doi.org/10.4269/ajtmh.2010.09-0373.

Mark, D.M., 1988. Network models in geomorphology. In: Modelling Geomorphological Systems. John Wiley, New York, USA.

Martinez, J.M., Le Toan, T., 2007. Mapping of flood dynamics and spatial distribution of vegetation in the Amazon floodplain using multitemporal SAR data. Remote Sens. Environ. 108 (3), 209–223. https://doi.org/10.1016/j.rse.2006.11.012.

Martz, L.W., Garbrecht, J., 1999. An outlet breaching algorithm for the treatment of closed depressions in a raster DEM. Comput. Geosci. 25 (7), 835–844. https://doi.org/10.1016/S0098-3004(99)00018-7.

Mason, D.C., Trigg, M., Garcia-Pintado, J., Cloke, H.L., Neal, J.C., Bates, P.D., 2016. Remote sensing of environment improving the TanDEM-X digital elevation model for flood modelling using flood extents from synthetic aperture radar images. Remote Sens. Environ. 173, 15–28. https://doi.org/10.1016/j.rse.2015.11.018.

Merwade, V., 2009. Effect of spatial trends on interpolation of river bathymetry. J. Hydrol. 371 (1–4), 169–181. https://doi.org/10.1016/j.jhydrol.2009.03.026. Elsevier B.V.

Merwade, V.M., Maidment, D.R., Goff, J.A., 2006. Anisotropic considerations while interpolating river channel bathymetry. J. Hydrol. 331 (3–4), 731–741. https://doi.org/10.1016/j.jhydrol.2006.06.018.

Merwade, V., Cook, A., Coonrod, J., 2008. GIS techniques for creating river terrain

models for hydrodynamic modeling and flood inundation mapping. Environ. Model. Softw. 23 (10 − 11), 1300–1311. https://doi.org/10.1016/j.envsoft.2008.03.005.
Neal, J., Schumann, G., Bates, P., 2012. A subgrid channel model for simulating river hydraulics and floodplain inundation over large and data sparse areas. Water Resour. Res. 48 (11), 1–16. https://doi.org/10.1029/2012WR012514.
O'Loughlin, F.E., Paiva, R.C.D., Durand, M., Alsdorf, D.E., Bates, P.D., 2016. A multi-sensor approach towards a global vegetation corrected SRTM DEM product. Remote Sens. Environ. 182, 49–59. https://doi.org/10.1016/j.rse.2016.04.018.
Paiva, R.C.D., Collischonn, W., Tucci, C.E.M., 2011. Large scale hydrologic and hydrodynamic modeling using limited data and a GIS based approach. J. Hydrol. 406 (3–4), 170–181. https://doi.org/10.1016/j.jhydrol.2011.06.007. Elsevier B.V.
Patel, A., Katiyar, S.K., Prasad, V., 2016. Performances evaluation of different open source DEM using differential global positioning system (DGPS). Egypt. J. Remote Sens. Space. Sci. 19 (1), 7–16. https://doi.org/10.1016/j.ejrs.2015.12.004.
Pekel, J.-F., Cottam, A., Gorelick, N., Belward, A.S., 2016. High-resolution mapping of global surface water and its long-term changes. Nature 540 (7633), 418–422. https://doi.org/10.1038/nature20584.
Planchon, O., Darboux, F., 2001. A fast, simple and versatile algorithm to fill the depressions of digital elevation models. Catena 46 (2–3), 159–176. https://doi.org/10.1016/S0341-8162(01)00164-3.
Rabus, B., Eineder, M., Roth, A., Bamler, R., 2003. The shuttle radar topography mission—a new class of digital elevation models acquired by spaceborne radar. ISPRS J. Photogramm. Remote Sens. 57 (4), 241–262. https://doi.org/10.1016/S0924-2716(02)00124-7.
Rodriguez, E., Morris, C., Belz, J., 2006. An assessment of the SRTM topographic products. Photogramm. Eng. Remote. Sens. 72 (3), 249–260 (doi:0099-1112/06/7203–0249/$3.00/0).
Sampson, C.C., Smith, A.M., Bates, P.D., Neal, J.C., Alfieri, L., Freer, J.E., 2015. A high-resolution global flood hazard model. Water Resour. Res. 51 (9), 7358–7381.
Sanyal, J., Carbonneau, P., Densmore, A.L., 2014. Low-cost inundation modelling at the reach scale with sparse data in the Lower Damodar River basin, India. Hydrol. Sci. J. 59 (12), 2086–2102. https://doi.org/10.1080/02626667.2014.884718. Taylor & Francis.
Senevirathne, N., Willgoose, G., 2013. A comparison of the performance of digital elevation model pit filling algorithms for hydrology. In: 20th International Congress on Modelling and Simulation. Adelaide, Australia, pp. 1624–1630. Available at: http://www.mssanz.org.au/modsim2013/H2/senevirathne.pdf.
Siart, C., Bubenzer, O., Eitel, B., 2009. Combining digital elevation data (SRTM/ASTER), high resolution satellite imagery (Quickbird) and GIS for geomorphological mapping: a multi-component case study on Mediterranean karst in Central Crete. Geomorphology 112 (1–2), 106–121. https://doi.org/10.1016/j.geomorph.2009.05.010.
Simard, M., Pinto, N., Fisher, J.B., Baccini, A., 2011. Mapping forest canopy height globally with spaceborne lidar. J. Geophys. Res. Biogeosci. 116 (November), 1–12. https://doi.org/10.1029/2011JG001708.
Smith, M.W., Macklin, M.G., Thomas, C.J., 2013. Hydrological and geomorphological controls of malaria transmission. Earth Sci. Rev. 116, 109–127. https://doi.org/10.1016/j.earscirev.2012.11.004. Elsevier B.V.
Sun, G., Ranson, K.J., Kharuk, V.I., Kovacs, K., 2003. Validation of surface height from shuttle radar topography mission using shuttle laser altimeter. Remote Sens. Environ. 88 (4), 401–411. https://doi.org/10.1016/j.rse.2003.09.001.
Tanis, F.J., Bourgeau-Chavez, L.L., Dobson, M.C., 1994. Application of ERS-1 SAR for coastal inundation. In: Proceedings of IGARSS '94 - 1994 IEEE International Geoscience and Remote Sensing Symposium. 3. pp. 1481–1483. https://doi.org/10.1109/IGARSS.1994.399475.
Tighe, M.L., Chamberlain, D., 2009. Accuracy comparison of the SRTM, ASTER, NED, NEXTMAP® USA digital terrain model over several USA study sites. In: DIGITAL MAPPING From Elevation to Information ASPRS/MAPPS 2009 Conference, pp. 12.
Tran, T.A., Raghavan, V., Masumoto, S., Vinayaraj, P., Yonezawa, G., 2014. A geomorphology-based approach for digital elevation model fusion - case study in Danang city, Vietnam. Earth Surf. Dyn. 2 (2), 403–417. https://doi.org/10.5194/esurf-2-403-2014.
Trigg, M.A., Bates, P.D., Wilson, M.D., Schumann, G., Baugh, C., 2012. Floodplain channel morphology and networks of the middle Amazon River. Water Resour. Res. 48 (10), 1–17. https://doi.org/10.1029/2012WR011888.
Twilley, R.R., 1985. An Analysis of Mangrove Forests Along the Gambia River Estuary: Implications for the Management of Estuarine Resources. (Michigan).
Vignolles, C., Lacaux, J.P., Tourre, Y.M., Bigeard, G., Ndione, J.A., Lafaye, M., 2009. Rift Valley fever in a zone potentially occupied by *Aedes vexans* in Senegal: dynamics and risk mapping. Geospat. Health 3 (2), 211–220. https://doi.org/10.4081/gh.2009.221.
Wang, L., Liu, H., 2006. An efficient method for identifying and filling surface depressions in digital elevation models for hydrologic analysis and modelling. Int. J. Geogr. Inf. Sci. 20 (2), 193–213. https://doi.org/10.1080/13658810500433453.
White, F., 1983. The vegetation of Africa: a descriptive memoir to accompany the UNESCO/AETFAT/UNSO vegetation map of Africa. Nat. Resour. Res. https://doi.org/10.2307/2260340.
Wilson, M., Bates, P., Alsdorf, D., Forsberg, B., Horritt, M., Melack, J., Frappart, F., Famiglietti, J., 2007. Modeling large-scale inundation of Amazonian seasonally flooded wetlands. Geophys. Res. Lett. 34 (15), 1–6. https://doi.org/10.1029/2007GL030156.
Wittmann, F., Junk, W.J., Piedade, M.T.F., 2004. The várzea forests in Amazonia: flooding and the highly dynamic geomorphology interact with natural forest succession. For. Ecol. Manag. 196 (2–3), 199–212. https://doi.org/10.1016/j.foreco.2004.02.060.
Yamazaki, D., Ikeshima, D., Tawatari, R., Yamaguchi, T., O'Loughlin, F., Neal, J.C., Sampson, C.C., Kanae, S., Bates, P.D., 2017. A high-accuracy map of global terrain elevations. Geophys. Res. Lett. 44 (11), 5844–5853. https://doi.org/10.1002/2017GL072874.
Yanlong, H., Xiuzhen, L., Craft, C., Zhigang, M., Yongguang, S., 2011. Relationships between vegetation zonation and environmental factors in newly formed tidal marshes of the Yangtze River estuary. Wetl. Ecol. Manag. 19 (4), 341–349. https://doi.org/10.1007/s11273-011-9220-8.
Yastikli, N., Koçak, G., Büyüksalih, G., 2006. Accuracy and morphological analyses of GTOPO30 and SRTM X–C Band DEMs in the test area istanbul. In: ISPRS Topographic Mapping from Space Workshop, pp. 6.
Zhang, Y., Xian, C., Chen, H., Grieneisen, M.L., Liu, J., Zhang, M., 2016. Spatial interpolation of river channel topography using the shortest temporal distance. J. Hydrol. 542, 450–462. https://doi.org/10.1016/j.jhydrol.2016.09.022.